NASA TN D-1435

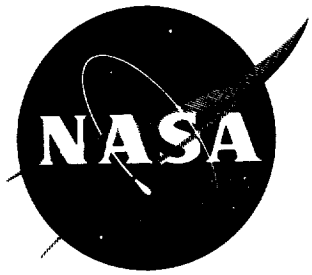

TECHNICAL NOTE

D-1435

HEAT-TRANSFER CHARACTERISTICS OF SEVERAL RADIATOR FINNED-TUBE CONFIGURATIONS

By E. M. Sparrow and W. J. Minkowycz

University of Minnesota,
Minneapolis, Minnesota

NATIONAL AERONAUTICS AND SPACE ADMINISTRATION

WASHINGTON

November 1962

NATIONAL AERONAUTICS AND SPACE ADMINISTRATION

TECHNICAL NOTE D-1435

HEAT-TRANSFER CHARACTERISTICS OF SEVERAL RADIATOR FINNED-TUBE CONFIGURATIONS

By E. M. Sparrow and W. J. Minkowycz

SUMMARY

An analytical study was performed to provide information on the heat loss to space from three radiator finned-tube configurations in which there is radiant interaction between fins and tubes. Numerical results for the heat-transfer characteristics of these configurations were obtained under the condition that the surfaces are blackbody radiators. A comparison showed the heat-loss results for the various configurations to be of very similar magnitude for equal fin weight. A method of analysis for the case of nonblack diffuse surfaces was also formulated.

INTRODUCTION

The use of radiating fins as a means for augmenting the heat-transfer performance of space radiators has received wide consideration in recent years. In response to the need for design information, analytical studies have been carried out to determine the rate of heat loss from fins to space under the combined action of surface radiation and internal heat conduction. The majority of such investigations has been concerned with fins that are essentially thin plates whose surfaces may radiate to space. Heat is transferred into such a fin by conduction through an edge that joins a tube within which flows a hot fluid.

In the initial studies of such plate fins, a simple model was adopted wherein the radiant interaction resulting from mutual irradiation between fin and tube was not included. References 1 and 2 are representative of several analytical treatments carried out along these lines. Radiators of practical interest, however, may consist of finned-tube configurations in which there is substantial radiant interaction between radiator elements. In practice, the detailed arrangement of fins and tubes in the radiator may be determined by considerations relating to fabrication, bonding, and assembly, to structural rigidity, and to meteoroid protection. Ultimate design decisions may be based on

a compromise among these several factors. It is therefore of interest to know the heat-transfer characteristics of a range of radiator configurations.

The aim of this investigation is to provide basic heat-transfer information for three finned-tube configurations, all of which involve radiant interaction between elements of the radiator. The analysis has been carried out with the dual purpose of providing specific information for each of the configurations and also of showing comparisons among the heat-transfer performances of the several configurations. Numerical results were obtained for the case in which the surfaces of the fins and tubes are blackbody radiators and the tubes are squared off. The method of analysis for nonblack surfaces is also formulated in detail.

Studies of plate fin and tube configurations that include radiant interaction between radiator elements are reported in references 3, 4, and 5. Unfortunately, the results of references 3 and 4 have to be regarded with some degree of uncertainty. This is because the angle factors in the radiant interchange analysis were not correctly derived. In addition, these references formulate the nonblack case by simply inserting factors of emissivity ϵ as multipliers of the emission and absorption terms that appear in the blackbody analysis. Such a treatment is only correct when there are no interreflections between the participating surfaces. When interreflections do occur, it is necessary to take account of the fact that the radiant flux leaving a surface location includes both reflected and emitted energy. Reference 5 is concerned only with the central fin-tube configuration. Numerical results are given for the case of black radiating surfaces. These results are not precisely comparable with those of this study inasmuch as the present analysis employs a squared-off model of the tube surface.

This research was sponsored by the National Aeronautics and Space Administration through the Office of Grants and Research Contracts.

SYMBOLS

A surface area

B radiosity, radiation leaving surface per unit time and area

F angle factor

H incident radiation per unit time and area

h	base surface height
k	thermal conductivity of fin
L	half-height of fin
$(N_c)_L$	conductance parameter based on dimension L, $\sigma T_b^3 L^2/kt$
Q	rate of heat loss to space from fin and from portions of base surface that interact with fin
T	absolute temperature
T_b	temperature of base surface
t	thickness of fin
X	dimensionless coordinate, x/L
x	position coordinate on fin
Y	dimensionless coordinate, y/L
y	position coordinate on fin
Z	dimensionless coordinate, z/h
z	position coordinate on base surface
α	absorptivity
β	dimensionless radiosity, $B/\sigma T_b^4$
ϵ	emissivity
θ	temperature variable, T/T_b
ρ	reflectivity
σ	Stefan-Boltzmann constant
$\varphi, \varphi', \varphi''$	angles defined in fig. 2

Subscripts:

b	base surface
c	due to conduction

f	fin
rad	radiation
s	space
1	base surface 1
2	base surface 2

GENERAL CONSIDERATIONS

The specific finned-tube configurations that will be considered in this investigation are pictured schematically in figure 1. In the left diagram of figure 1(a), the tubes are contained between a pair of plane, plate fins. This arrangement will be designated herein as the closed-sandwich configuration. In practice, it will neither be possible nor desirable to have a small region of contact between the tube and the fin. Such a limited contact would give rise to a large thermal resistance tending to inhibit heat flow from the tube into the fin. It would appear desirable to employ fillets of high-thermal-conductivity material to increase the area of contact. This suggests that a suitable model for analytical treatment of the radiant interchange within the space between the fins might be a squared-off tube. This idea has been adopted herein and is pictured in the right diagram in figure 1(a). The second configuration to be considered is similar to that already discussed, except that one plate is removed. This is pictured in figure 1(b), with the left diagram showing circular tubes and the right diagram the model adopted in the analysis. This assembly will be designated as the open sandwich. The last of the configurations that will be analyzed is the central fin and tube radiator, which is pictured at the left in figure 1(c). To permit meaningful comparisions with the prior cases, a squared-off model of the central fin will be employed as shown at the right in figure 1(c).

The length of the various finned-tube assemblies in the direction normal to the plane of figure 1 is sufficiently great so that end effects need not be included in the derivation of the radiation angle factors. Additionally, temperature variations in this direction are also assumed sufficiently gradual so as to maintain the two-dimensional character of the problem.

Dimensional nomenclature and coordinates appropriate to the analysis are shown in figure 1. The squared-off tube surface, hereinafter called the base surface, is assumed to have a uniform temperature T_b.

If consideration is given to the parameters that govern the heat transport, it is found that, after dimensionless variables have been formed, there emerge:

$$L/h, \quad (N_c)_L = \sigma T_b^3 L^2/kt \tag{1}$$

The first of these is purely geometrical and governs the aspect ratio of the cavity formed by the fins and tubes. The N_c parameter is essentially a ratio of thermal conductances, comparing the radiation capability at the surface with the heat conducting capability of the fin. For highly conducting fins, N_c is very close to zero; for lesser conducting fins, N_c takes on larger values. Hereinafter, N_c will be termed the conductance parameter.

The number of emissivities ϵ and absorptivities α that enter the problem depends on the details of the particular system. The radiation properties of the base surface may either be different from or the same as those of the fins. There may or may not be a difference between the radiation characteristics of surfaces radiating to space and those radiating internally. If radiation from an external source such as the sun is involved, the absorptivity for solar radiation may be different from that for infrared radiation. The description of radiation from an external source would involve at least two additional parameters, one for the magnitude of the incoming energy and a second for its angle of incidence.

In view of the large number of parameters, it is clear that an attempt at a completely general treatment would involve a massive computational effort, especially since numerical solutions of nonlinear, integrodifferential equations are required. This suggests that the role of each parameter be carefully reconsidered. In this connection, it is reasonable to expect that surface materials having the highest practically obtainable emissivity will be used. Such emissivities may very likely be attained by the use of coatings. Thus, in practice, the emissivity should not differ too much from that of a black surface. With this in mind, the main emphasis of this study will relate to black surfaces, and this is the condition for which numerical results will be obtained. The use of black surfaces results in a computational problem much more tractable than that encountered when nonblack surfaces are used. However, for completeness, a formulation of the problem for nonblack surfaces will be carried out in the appendix. In addition to the condition of black surfaces, the present analysis will also be confined to the situation in which radiation from an external source is negligible compared with energy emitted by the finned-tube system.

TEMPERATURE DISTRIBUTION

Governing Equation

In carrying out the analysis, it will be convenient to begin with the closed-sandwich configuration shown in figure 1(a). Once the governing equation for the temperature distribution has been formulated for this case, only simple modifications need be made to obtain the corresponding equations for the other configurations.

Closed-sandwich configuration. - The analysis begins with the application of the conservation-of-energy principle to an elementary volume of fin, which is shown as shaded in figure 2. Under steady-state conditions, the net outflow of energy from such an element must be zero; therefore,

$$(dQ_{net})_c + (dQ_{net})_{rad} = 0 \tag{2}$$

For a thin (one-dimensional) fin, the net outflow of heat due to conduction is

$$(dQ_{net})_c = -kt \frac{d^2T}{dx^2} dx \tag{3}$$

per unit length normal to the plane of the figure. The net outflow of radiant energy is the difference between the emitted and the incident radiation. The radiant emission is given by the Stefan-Boltzmann law as $\left[\sigma T^4(x)\right] 2\ dA_x$, in which the factor 2 is introduced because both surfaces of the element are emitting. With this, the net radiation may be written

$$(dQ_{net})_{rad} = \left[2\sigma T^4(x) - H(x)\right] dA_x \tag{4}$$

where H denotes the incident energy falling upon x per unit time and area.

The incident radiation comes from two distinct zones: (1) from the opposite fin, and (2) from the base surfaces. The contribution from the opposite fin will be derived first. Consider radiation leaving a typical surface element of the opposite fin, say dA_y. This element is in reality a narrow strip, having a dimension dy in the plane of figure 2, but extending to infinity in both directions normal to the plane of the figure. The energy emitted by dA_y is $\left[\sigma T^4(y)\right] dA_y$, and this is distributed over all directions in space. Of this, an

amount $\sigma T^4(y)dA_y\, dF_{dA_y\text{-}dA_x}$ is incident on dA_x, where $dF_{dA_y\text{-}dA_x}$ is an angle factor for diffuse interchange. However, by the reciprocity rule for diffuse angle factors, $dA_y\, dF_{dA_y\text{-}dA_x} = dA_x\, dF_{dA_x\text{-}dA_y}$. With this, the contribution of dA_y to the incident energy at dA_x is $\sigma T^4(y)dA_x\, dF_{dA_x\text{-}dA_y}$; but such contributions arrive from all locations on the opposite fin, and the total amount is found by integration:

$$dA_x \int_{y=0}^{2L} \sigma T^4(y) dF_{dA_x\text{-}dA_y} \tag{5}$$

The radiation incident at dA_x from the base surfaces may be derived in a similar manner. The final expressions are most easily obtained by modifying equation (5). Since the base surface temperature is uniform, it may be removed from under the integral sign. Additionally, the integral of an infinitesimal angle factor yields a finite angle factor. Applying this to the two base surfaces 1 and 2 (fig. 2) gives

$$dA_x \sigma T_b^4 \left(F_{dA_x\text{-}1} + F_{dA_x\text{-}2}\right) \tag{6}$$

With expressions (5) and (6), the radiant energy $H(x)$ incident per unit area at x is

$$H(x) = \int_{y=0}^{2L} \sigma T^4(y) dF_{dA_x\text{-}dA_y} + \sigma T_b^4 \left(F_{dA_x\text{-}1} + F_{dA_x\text{-}2}\right) \tag{7}$$

The net radiation may then be found by substituting $H(x)$ into equation (4). Thus, with both the net radiation and net conduction available, the energy balance equation (2) may be evaluated. This gives

$$kt \frac{d^2T}{dx^2} = 2\sigma T^4(x) - \int_{y=0}^{2L} \sigma T^4(y) dF_{dA_x\text{-}dA_y} - \sigma T_b^4 \left(F_{dA_x\text{-}1} + F_{dA_x\text{-}2}\right) \tag{8}$$

Introducing the dimensionless variables

$$X = x/L, \qquad Y = y/L, \qquad \theta = T/T_b \tag{9}$$

equation (8) becomes

$$\frac{d^2\theta}{dX^2} = (N_c)_L \left[2\theta^4(X) - \int_{Y=0}^{2} \theta^4(Y) dF_{dA_x - dA_y} - \left(F_{dA_x - 1} + F_{dA_x - 2} \right) \right] \tag{10}$$

in which the conductance parameter N_c has already been defined by equation (1). Because of the symmetry of the problem, it is clear that $\theta(X)$ and $\theta(Y)$ are the same functions; only the independent variables have been interchanged. Thus, equation (10) is an integrodifferential equation for θ. Since both θ and θ^4 appear, the equation is nonlinear.

To complete the specification of the problem, the boundary conditions must be stated and expressions must be provided for the angle factors that appear in equation (10). One of the boundary conditions is that $T = T_b$ at $x = 0$. Additionally, there is a symmetry condition at $x = L$, the mathematical representation of which is $dT/dx = 0$. In dimensionless terms, these are

$$\theta(0) = 1 \qquad (d\theta/dX)_{X=1} = 0 \tag{11}$$

In the derivation of the angle factors, it is advantageous to make use of special properties associated with surfaces that have one elongated dimension (essentially infinite normal to the plane of fig. 2). In general, the angle factor between an element dA_x and an <u>infinite strip</u> dA_y is (ref. 6)

$$dF_{dA_x - dA_y} = \frac{1}{2} \frac{d}{dy} (\sin \varphi) dy \tag{12}$$

wherein the angle φ is defined by the normal to dA_x and the connecting line between dA_x and dA_y as shown in figure 2. From the geometry of the figure

$$\sin \varphi = (y - x)/\sqrt{(y - x)^2 + h^2}$$

Carrying out the indicated differentiation results in

$$dF_{dA_x\text{-}dA_y} = \frac{\frac{1}{2}\left(\frac{h}{L}\right)^2}{\left[(Y - X)^2 + \left(\frac{h}{L}\right)^2\right]^{3/2}} dY \tag{13}$$

For interchange between dA_x and an infinite strip that spans a finite dimension in the plane of the figure, a generalization of equation (12) may be applied. For instance, for the angle factor to the base surface 2,

$$F_{dA_x\text{-}2} = \frac{1}{2}(\sin \varphi'' - \sin \varphi') \tag{14}$$

where φ'' and φ' are defined in the lower sketch of figure 2. When equation (14) is evaluated and dimensionless variables are introduced,

$$F_{dA_x\text{-}2} = \frac{1}{2}\left\{1 - \frac{(2 - X)}{\left[(2 - X)^2 + \left(\frac{h}{L}\right)^2\right]^{1/2}}\right\} \tag{15}$$

Similarly, for the base surface 1,

$$F_{dA_x\text{-}1} = \frac{1}{2}\left\{1 - \frac{X}{\left[X^2 + \left(\frac{h}{L}\right)^2\right]^{1/2}}\right\} \tag{16}$$

With the foregoing formulation of the angle factors, the evaluation of the energy conservation principle is now complete. There is, however, one additional simplification that may be introduced into equation (10). This results from the symmetry of the temperature distribution about $x = L$; that is, $T(x) = T(2L - x)$. When this symmetry property is incorporated into equation (10) along with the appropriate angle factors, there follows

$$\frac{1}{(N_c)_L}\frac{d^2\theta}{dX^2} = 2\theta^4(X) - \frac{\left(\frac{h}{L}\right)^2}{2}\int_0^1 \theta^4(Y)dY\left\{\frac{1}{\left[(Y - X)^2 + \left(\frac{h}{L}\right)^2\right]^{3/2}} + \frac{1}{\left[(2 - Y - X)^2 + \left(\frac{h}{L}\right)^2\right]^{3/2}}\right\}$$

$$- 1 + \frac{1}{2}\left\{\frac{X}{\left[X^2 + \left(\frac{h}{L}\right)^2\right]^{1/2}} + \frac{2 - X}{\left[(2 - X)^2 + \left(\frac{h}{L}\right)^2\right]^{1/2}}\right\} \tag{17}$$

Inspection of equation (17) reveals that there are two independent parameters that must be specified for each solution: the conductance parameter N_c and the aspect ratio h/L. Further study indicates that analytical solutions cannot be achieved, and numerical means must be employed. The numerical solutions will be discussed after the governing equations for the other configurations have been derived.

Open-sandwich configuration. - The energy equation for the open-sandwich configuration is most conveniently derived by modifying the foregoing analysis for the closed sandwich. In fact, for the open sandwich, it is only necessary to delete the terms that describe the radiant interaction between the fins - the integral terms appearing in equation (17). With this modification, the governing equation for the fin-temperature distribution in the open-sandwich configuration becomes

$$\frac{1}{(N_c)_L}\frac{d^2\theta}{dX^2} = 2\theta^4(X) - 1 + \frac{1}{2}\left\{\frac{X}{\left[X^2 + \left(\frac{h}{L}\right)^2\right]^{1/2}} + \frac{2 - X}{\left[(2 - X)^2 + \left(\frac{h}{L}\right)^2\right]^{1/2}}\right\} \qquad (18)$$

The boundary conditions remain as stated in equation (11).

By comparing equation (18) for the open sandwich with equation (17) for the closed sandwich, a very significant mathematical difference is apparent; namely, the former is a differential equation, while the latter is an integrodifferential equation. In general, differential equations are easier to solve than integrodifferential equations. While equation (18) is, in fact, simpler than equation (17), numerical solutions are still required. These will be discussed later.

Central-fin configuration. - The energy equation for the central fin may, in turn, be derived by modifying equation (18) for the open sandwich. The aspect requiring modification is the interchange between the fin and base surfaces. For the central-fin configuration, the interchange occurs between dA_X and a wall of height $h/2$ (assuming $t << h$) rather than of height h as in the open sandwich. Thus, wherever h appears in equation (18), it is replaced by $h/2$. Additionally, both the upper and lower sides of the central fin exchange heat with the base surfaces, which requires that a multiplying factor of 2 be inserted in

the angle factor terms of equation (18). When these modifications are made, the revised form of equation (18) now applicable to the central-fin configuration is

$$\frac{1}{(N_c)_L}\frac{d^2\theta}{dX^2} = 2\theta^4(X) - 2 + \frac{X}{\left[X^2 + \left(\frac{h}{2L}\right)^2\right]^{1/2}} + \frac{2 - X}{\left[(2 - X)^2 + \left(\frac{h}{2L}\right)^2\right]^{1/2}} \tag{19}$$

The boundary conditions of equation (11) continue to apply. Numerical solutions of equation (19) will be discussed in the following paragraphs.

Solutions

Method. - As has already been indicated, it was necessary to use numerical techniques to solve the foregoing equations for θ. The numerical solutions were carried out on a Univac 1103 electronic digital computer. The procedure for solving equation (17) will be described first. In essence, a weighted iteration technique was employed. The first step was to prescribe the parameters N_c and L/h; then, a trial distribution of $\theta(Y)$ was selected. For a fixed value of X, the integral appearing on the right side of equation (17) was carried out numerically. Then, another value of X was chosen and the integral was carried out once again, and so forth. In this way, corresponding to the particular θ function, a value of the integral was generated at every mesh point X in the range $0 \leq X \leq 1$. This set of values may be denoted by $f(X)$, while the remaining terms on the right side, aside from θ^4, may be denoted by $g(X)$. Thus, equation (17) may be written as

$$\frac{d^2\theta}{dX^2} = (N_c)_L \left[2\theta^4 + f(X) + g(X)\right] \tag{20}$$

Integration of equation (20) subject to the boundary conditions (11) leads to

$$\theta(X) = 1 + 2(N_c)_L \int_0^X \left(\int_0^X \theta^4 \, dX - \int_0^1 \theta^4 \, dX \right) dX$$

$$+ (N_c)_L \int_0^X \left\{ \int_0^X \left[f(X) + g(X) \right] dX - \int_0^1 \left[f(X) + g(X) \right] dX \right\} dX \qquad (21)$$

As previously described, $f(X)$ is available for a particular trial distribution of θ, while $g(X)$ is a known function of X. Therefore, the integration indicated in the last term of equation (21) can be carried out numerically. Also, by utilizing the trial distribution of θ, the integrals involving θ^4 may also be carried out. By these calculations, a new θ distribution is generated from equation (21).

In a direct iteration scheme, the new trial function would serve as input to the next cycle of calculations. However, in a nonlinear system, direct iteration may often lead to divergence rather than convergence. The procedure used herein was to take the input and output θ functions, which may be respectively denoted by θ_n and θ_{n+1}, and form their difference. The trial function θ^* for the next cycle of calculations was then constructed as

$$\theta^* = \theta_n + \lambda(\theta_{n+1} - \theta_n) \qquad 0 \leq \lambda \leq 1$$

The size of λ could be controlled manually from the console of the computer. An on-line typewriter printed out $\int_0^1 (\theta_{n+1} - \theta_n) dX$, and adjustments could be made in λ if the trend of this integral indicated divergence. In general, cases characterized by small L/h could be run at λ values near 1, while cases at large L/h required smaller λ values to ensure convergence (as low as $\lambda = 0.1$).

Solutions were obtained for L/h values of 1/2, 1, 2, 3, 4, and 5 for each of which parametric values of N_c were selected in the range from 0 to 10. In all, 56 cases were solved for the closed-sandwich configuration.

The same basic procedure was employed to find solutions of equations (18) and (19), respectively, for the open sandwich and the central fin. However, there was one major simplification that resulted from the fact that these equations are differential rather than integrodifferential; namely, the $f(X)$ no longer appears in equation (21). The fact that it was no longer necessary to compute $f(X)$ enabled the solutions for equations (18) and (19) to be carried out more rapidly than those for equation (17). The same parameter ranges were covered in the solutions of equations (18) and (19), as have already been discussed in connection with the solutions of equation (17).

Results. - Each solution of the energy equations (17) to (19) provides a distribution of temperature along the fin. In view of the large number of cases that has been considered, it is neither possible nor necessary to present temperature profiles for all. Instead, a representative set of profiles will be presented for each of the radiator configurations. These results are plotted in figure 3 for the closed-sandwich, open-sandwich, and central-fin configurations. On each figure curves are given for T/T_b as a function of position x/L for parametric values of N_c and L/h.

Figure 3(a) shows that the temperature drop along the fin is very small when N_c is very small (see, e. g., the curves for $N_c = 0.25$). This is due to the low thermal resistance of the fin. Additionally, there is very little effect of L/h when N_c is small, although it is clear that the temperature drop is greater as L/h increases. As N_c increases, so also does the temperature drop along the fin. The effect of L/h also becomes much more marked at the higher N_c values. For a given value of N_c, it has been verified that the temperature profile for the single, noninteracting fin falls slightly below that for $L/h = 5$. This is fully plausible, since the noninteracting fin is equivalent to the case of $L/h = \infty$.

The trends just enumerated for the closed sandwich are also in evidence in figures 3(b) and (c), which correspond respectively to the open sandwich and the central fin. The curves on these latter two figures fall somewhat lower than those of figure 3(a) because, for a given N_c value, there is twice as much fin volume in the closed-sandwich configuration as there is in the open sandwich or the central fin.

The figures generally show that, when N_c is high, the temperatures in the central region of the fin are quite low. When it is recalled that the emission is proportional to the fourth power of the temperature, it is clear that the fin material in the central region is of marginal utility. The presence of a larger base surface (smaller L/h) tends to raise the temperature in the central region, making this part of the fin more useful.

HEAT TRANSFER

Heat-transfer results based on the foregoing numerical solutions will now be presented and discussed for the separate configurations. Comparisons among these results will then be made. A superposition calculation of the heat loss will also be explored.

Heat-Transfer Characteristics

The heat-transfer results to be presented here will include the heat loss to space from the fin and from those portions of the base surface that interact radiatively with the fin. The heat loss from those portions of the base surface that radiate directly to space without interaction will not be included. In this latter category fall the upper and lower surfaces of the squared-off tubes, that is, the horizontal surfaces of the squared-off tubes as they are pictured in figure 1. The heat loss from such surfaces is simply σT_b^4 times their surface area, and this may be added at any time to the results presented herein.

Closed-sandwich configuration. - When excluding the noninteracting portions of the squared-off tube as discussed previously, the heat loss to space from the closed-sandwich configuration is due to radiation from the surface of the fin. The rate of heat loss from the fin surface per unit area at x is $\sigma T^4(x)$. The overall rate of heat loss Q from the pair of fins that forms the sandwich is

$$Q = 2\int_0^{2L} \sigma T^4(x)\,dx \tag{22}$$

per unit length normal to the plane of figure 1. In dimensionless terms, this becomes

$$\frac{Q}{4L\sigma T_b^4} = \int_0^1 \theta^4(X)\,dX \tag{23}$$

in which the symmetry of θ about $x = L$ has been taken into account. The group $4L\sigma T_b^4$ is the heat loss from the fins under the condition that their temperature is uniform at the value T_b. Such a condition can be achieved only by fins of infinite thermal conductivity ($N_c = 0$).

Therefore, $4L\sigma T_b^4$ represents the largest possible heat loss from the system. The ratio expressed by equation (23) thus compares the actual heat loss with the ideal heat loss. Such a ratio may be regarded as an effectiveness of the system.

The effectiveness ratio represented by equation (23) has been evaluated by numerical integration of the previously discussed temperature solutions. The results thus obtained are presented in figure 4 as a function of N_c for parametric values of the aspect ratio L/h. Inspection of the figure reveals that for any fixed L/h the heat loss from the system decreases with increasing values of N_c. This trend is in complete accord with physical reasoning, since an increase in N_c is an indication of an increase in the thermal resistance of the fin (because of a decrease in thermal conductivity k or fin thickness t). The sharpest decrease in fin heat loss occurs at small values of N_c.

It may additionally be seen from the figure that the effectiveness decreases monotonically with increasing L/h. Since L appears in the ordinate variable as well as in L/h, this trend may be most conveniently discussed by supposing L to be fixed. Then, an increase in L/h corresponds to a decrease in the separation h between the fins. In particular, the case of $L/h = \infty$ corresponds to the situation in which the separation h vanishes, and the pair of fins forming the sandwich coalesces into a single fin of thickness $2t$. Thus, the heat-loss results for the $L/h = \infty$ case are identical to those for a single, isolated fin of thickness $2t$. These isolated fin results were taken from reference 5.

To explain why the heat loss decreases with decreasing h (fixed L), it is first necessary to describe the role of radiation within the cavity of the closed-sandwich configuration. This radiation provides a means of transport between the fins and the base surfaces and between high- and low-temperature portions of the fin, which is in addition to the heat conduction in the fin. In effect, the internal radiation and the conduction are parallel heat-flow paths. Thus, the presence of the internal radiation is equivalent to an increase in the thermal conductivity of the fin. The most important transport of radiation within the cavity takes place between the base surfaces and the fins. Either by physical reasoning or by inspection of equations (15) and (16), it is easy to see that the transport between fin and base surface decreases as the spacing h decreases. Additionally, from equation (13), it is also seen that the transport between widely separated locations on the fins (i.e., Y substantially different from X) decreases as h decreases. Thus, internal radiation becomes less effective as a transport mechanism as h decreases. The trend among the curves of figure 4(a) showing Q decreasing with decreasing h (fixed L) is thus made plausible.

It is interesting to inquire about the quantitative relation between internal radiation and fin heat conduction, the sum of which constitutes the total heat loss. The heat conducted into the fin at the base Q_c was calculated by Fourier's law:

$$Q_c = -kt(dT/dx)_{x=0} \tag{24}$$

This equation was placed in dimensionless form and then evaluated from the solutions of the energy equation (17). The ratio of Q_c to the total heat loss Q has been constructed, and the results are plotted in figure 5. It is clearly seen from the figure that the importance of heat conduction in the fin relative to internal radiation decreases as L/h decreases. This is in accordance with the discussion of the preceding paragraph. Additionally, it is seen that heat conduction is the dominant heat-transfer path at low values of N_c and that internal radiation grows increasingly important as N_c increases. This follows from the fact that small values of N_c indicate small thermal resistance for heat conduction in the fin.

Open-sandwich configuration. - From a consideration of the right diagram of figure 1(b), it is clear that there is a heat loss to space both from the fin and from the vertical base surface walls that interact with the fin. The net heat loss from the fin (both sides) is equal to the heat conducted into the fin. From Fourier's law

$$Q_f = 2\left[-kt(dT/dx)_{x=0}\right] \tag{25a}$$

in which the factor of 2 is included because there is an inflow at both $x = 0$ and at $x = 2L$. In dimensionless terms, this is

$$\frac{Q_f}{4L\sigma T_b^4} = \frac{1}{2(N_c)_L}\left(-\frac{d\theta}{dX}\right)_{X=0} \tag{25b}$$

The net heat loss from the base surface is equal to the energy emitted by the surface minus the incident radiant flux. The emission is simply $\sigma T_b^4 h$ per unit length normal to the plane of the figure. The incident radiation originates at the fin and at the opposite base surface. In mathematical terms, the net base surface heat loss is

$$Q_b = 2\left[\sigma T_b^4 h - \int_0^{2L} \sigma T^4(x) F_{dA_x-1}\, dx - \sigma T_b^4 h F_{1-2}\right] \tag{26a}$$

in which the factor of 2 is included because two base surfaces are involved. By introducing dimensionless variables, this becomes

$$\frac{Q_b}{4L\sigma T_b^4} = \frac{1}{2}\left[\frac{h}{L}(1 - F_{1-2}) - \int_0^2 \theta^4(X) F_{dA_x-1}\, dX\right] \tag{26b}$$

The angle factor F_{dA_x-1} is already available in equation (16), while the angle factor F_{1-2} for interchange between two parallel surfaces follows from reference 6 (eq. (31-49)) as

$$F_{1-2} = \sqrt{\left(\frac{2L}{h}\right)^2 + 1} - \frac{2L}{h} \tag{27}$$

The total heat loss Q from the system is found by adding Q_b and Q_f:

$$\frac{Q}{4L\sigma T_b^4} = \frac{Q_f}{4L\sigma T_b^4} + \frac{Q_b}{4L\sigma T_b^4} \tag{28}$$

As written in equation (28), Q is expressed as a ratio with the quantity $4L\sigma T^4$ as with the closed sandwich. It will now be shown that $4L\sigma T_b^4$ is precisely equal to the maximum possible heat loss from the system. For the case of infinite thermal conductivity ($N_c = 0$), the fin temperature is uniform; that is, $\theta = 1$ throughout. In this instance, Q_b can be evaluated from equation (26b) by removing θ from under the integral sign. Additionally,

$$\frac{1}{2}\int_0^2 F_{dA_x-1}\, dX = F_{f-1}$$

where F_{f-1} is the angle factor from the fin to the base surface 1. Thus,

$$\frac{Q_b}{4L\sigma T_b^4} = \frac{h}{2L}(1 - F_{1-2}) - F_{f-1} \tag{29}$$

But, by angle factor algebra, $F_{1-2} + F_{1-f} + F_{1-s} = 1$, in which F_{1-s} indicates the angle factor from the base surface 1 to space. Clearly, because of symmetry, $F_{1-s} = F_{1-f}$. Also, from the reciprocity theorem for diffuse angle factors, $2LF_{f-1} = hF_{1-f}$. Incorporating this into equation (29), there follows

$$\frac{Q_b}{4L\sigma T_b^4} = \frac{h}{2L} F_{1-f} \tag{30}$$

It is to be remembered that this applies for the limiting situation where the fin is isothermal ($N_c = 0$). The fin heat loss for this limiting situation cannot be calculated from equation (25a) because k is infinite and $d\theta/dX$ is zero. Instead, Q_f is determined as the difference between the emitted and incident radiation. For the fin at uniform temperature T_b, this is

$$Q_f = 2\left(2L\sigma T_b^4 - h\sigma T_b^4 F_{1-f}\right) \tag{31}$$

or

$$\frac{Q_f}{4L\sigma T_b^4} = 1 - \frac{h}{2L} F_{1-f} \tag{32}$$

Now, adding equations (30) and (32) to find the total rate of heat loss gives

$$Q = 4L\sigma T_b^4 \tag{33}$$

This is the maximum possible heat loss from the system. Thus, the ratio expressed by equation (28) is the effectiveness of the system as in the case of the closed sandwich.

Values of the effectiveness have been determined by numerically evaluating equations (25b) and (26b) in conjunction with the θ solutions of equation (18). The results thus obtained have been plotted in

figure 6 as a function of N_c for parametric values of the aspect ratio L/h. The general trends that have been discussed in connection with figure 4 for the closed-sandwich configuration are also in evidence in figure 6 for the open-sandwich configuration. However, there are certain interesting differences in detail. The decrease in Q with increasing L/h (decreasing h) is much sharper for the open sandwich than for the closed sandwich. In considering this result, it should be noted that for a given fin thickness t there is only half as much fin volume in the open-sandwich configuration as there is in the closed-sandwich configuration. Consequently, there is less cross-sectional area for heat conduction in the open sandwich. It is therefore reasonable that the open sandwich should be more sensitive to the effects of internal radiation than the closed sandwich. Consequently, as the internal radiation diminishes with decreasing h, the heat loss Q will be more affected for the open sandwich than for the closed sandwich. Comparison of numerical values between figures 6 and 4 will be reserved until later.

It is also of interest to know what fraction of the overall heat loss is transferred from the fin and what fraction is from the interacting portion of the base surface. This information is obtained directly from equations (25b) and (26b) for $N_c > 0$; for $N_c = 0$, equations (30) and (32) are used. A plot of Q_f/Q is presented in figure 7. Corresponding results for Q_b/Q may be readily obtained by applying the relation $Q_b/Q = 1 - (Q_f/Q)$. Inspection of the figure reveals that the fin's fraction of the total heat loss is greatest for large values of L/h and small values of N_c. The trend of Q_f/Q increasing with increasing L/h is related to the increase in fin surface area relative to the base surface area. On the other hand, the changes in Q_f/Q with N_c are due to changes in fin temperature distribution. For small values of N_c, temperatures throughout the fin are relatively high, and the fin heat loss is correspondingly high. For high values of N_c, the fin temperature drops off rapidly with increasing distance from the base surface, and, as a consequence, the fin heat loss is low.

The open-sandwich configuration pictured in figure 1(b) is unsymmetrical in that the lower surface is a plane sheet, while the upper surface is, in essence, a cavity. The vertical walls of the cavity are at the temperature T_b, which is the highest temperature in the system. It would therefore be expected that the heat loss to space from the cavity side would exceed that from the plane side. It is of interest to explore the relation between these heat losses quantitatively. The heat loss to space from the plane side of the configuration is given by

$$Q_{\text{plane side}} = \int_0^{2L} \sigma T^4(x)\,dx \tag{34}$$

Numerical results have been obtained by evaluating the integral with the θ solutions of equation (18). The ratio of the heat loss from the plane side to the total heat loss Q has been constructed, and the results are presented in figure 8 as a function of N_c for parametric values of the aspect ratio L/h. As expected, the heat loss from the plane side is less than one-half of the total (except in the limit at $N_c = 0$). From the figure, it is seen that, as the L/h ratio increases, the heat losses from the plane and cavity sides tend to equalize (i.e., the ratio plotted in fig. 8 approaches more closely to one-half). This is due to the fact that the base surfaces play a less important role as L/h increases (h decreases). Further study reveals that the unbalance in heat loss between the cavity and plane sides is accentuated at high values of N_c. Large values of N_c are effective in diminishing the fin heat loss relative to the base surface heat loss. Thus, at large N_c, the cavity side is favored by virtue of the presence of the base surfaces.

Central-fin configuration. - In common with the open sandwich, the heat loss to space from the central-fin configuration takes place in part from the fin and in part from the base surfaces. The net heat loss from the fin is expressed as before by equation (25b). On the other hand, the net base surface heat loss as given by equation (26a) must be somewhat modified to take account of geometrical differences between the open-sandwich and central-fin configurations. Figures 1(b) and (c) show that the radiant interchange in the central-fin configuration involves base surface elements of length $h/2$ instead of length h as for the open sandwich. Additionally, there are now four participating base surface elements rather than two as in the previous case. When these modifications are incorporated into equation (26a), it is found that the dimensionless base surface heat loss is expressed by

$$\frac{Q_b}{4L\sigma T_b^4} = \frac{1}{2}\left[\frac{h}{L}\left(1 - F_{1-2}\right) - 2\int_0^2 \theta^4(X) F_{dA_X-1}\, dX\right] \tag{35a}$$

in which

$$F_{1-2} = \sqrt{\left(\frac{4L}{h}\right)^2 + 1} - \left(\frac{4L}{h}\right) \tag{35b}$$

$$F_{dA_X-1} = \frac{1}{2}\left\{1 - \frac{X}{\left[X^2 + (h/2L)^2\right]^{1/2}}\right\} \tag{35c}$$

The overall rate of heat loss from the system is found by adding the contributions of the fin and of the base surfaces. Numerical values have been obtained by evaluating equations (25b) and (35a) in conjunction with the temperature solutions of equation (19). The heat-loss results thus calculated have been plotted in figure 9 as a function of N_c for parametric values of the aspect ratio L/h. The overall appearance of this figure and the general trends among the results are quite similar to those already enumerated and discussed in connection with figure 6 and, therefore, need not be repeated. A numerical comparison of the heat-loss results of figure 9 with those of figures 6 and 4 will be made in the forthcoming section.

Inasmuch as there is a heat loss to space from both fin and base, it is of interest to inquire about the relative importance of each. The fin heat loss has been calculated from equation (25b), and, with this information, the ratio Q_f/Q has been constructed. The results are plotted in figure 10, where it is seen that the fin's contribution to the overall heat loss is greater for large L/h and for small N_c. The explanation of these trends has already been discussed in connection with figure 7. A numerical comparison of figures 10 and 7 shows that, for large L/h, there is little difference between the Q_f/Q values for the open sandwich and for the central fin. This is fully plausible inasmuch as the base surface plays only a minor role when L/h is large. The detailed arrangement of fin and base surface should therefore have little effect. On the other hand, there are larger departures between the two sets of results at small L/h, with the Q_f/Q values for the open sandwich (fig. 7) being higher than those for the central fin (fig. 10).

Comparison on Basis of Equal Fin Weight

The foregoing presentation of results has been focused on the heat-transfer characteristics of each of the specific configurations under study. Now, consideration will be given to a comparison of the heat-transfer performance of these configurations. As a basis for the comparison, the condition of equal fin weight has been selected here. Other bases of comparison for the complete radiator configuration are possible, one of which might be equal radiator (tube plus fin) weight, but this involves variables such as tube wall thickness that are not among the parameters of this study.

Referring to figure 1, it is clear that the condition of equal fin weight is achieved when the thickness of each of the fins comprising the closed sandwich is one-half that of the fins in the other configurations. The fin thickness enters the analysis only in the N_c parameters (see eq. (1)). Thus, for a comparison at equal fin weight, the

N_c parameter for the closed-sandwich configuration should be taken twice as large as the N_c parameter for the other two configurations.

A comparison of the heat-loss characteristics of the various fin-tube configurations is presented in figure 11. This figure is subdivided into several graphs, with each graph corresponding to a fixed fin weight. There are three curves in each graph to represent the results for each of the three configurations. Figure 11(a) contains comparisons for the lower N_c values, while figure 11(b) is for the higher N_c values. The abscissa variable for all the graphs is L/h.

Inspection of the figures shows that the major differences in heat-transfer performance among the various configurations occur at small values of L/h. This occurrence may be understood by recalling that the importance of the base surface heat loss is greatest when L/h is small. Therefore, it is natural that the details of the base surface arrangement should be important for small L/h. As L/h increases, it is seen from the graphs that the spread among the curves diminishes. In practice, it would be expected that L/h values in excess of three would be most probable. In such an event, the performance differences among the configurations are quite moderate. For example, in the middle graph of figure 11(a), which represents a practically realistic level of N_c, the overall spread among the curves is about 3 percent at $L/h = 3$.

Generally speaking, the spread among the curves grows larger on a percentage basis as the level of N_c increases. This is related to the increasing role of the base surface with increasing N_c. The N_c values of figure 11(a) lie in the range of current practical interest, while those of figure 11(b) are somewhat on the high side.

The open-sandwich configuration appears to show the best heat-transfer characteristics among the various configurations studied here. However, except at low values of L/h, the margin of difference is not decisive.

Superposition of Results for Noninteracting Surfaces

The heat-transfer results that have been presented in this report have been derived from rather lengthy numerical solutions. It is worthwhile inquiring whether a close approximation to these results can be achieved by a combination of other, more easily derivable results. In this connection, it is natural to take as a starting point the heat-loss results for the single, noninteracting fin. These results are readily available in the open literature (e.g., in refs. 1 and 2). To these results for the noninteracting fin should be added a quantity that characterizes the heat loss of the base surface and, in particular, that part of the base surface that interacts with the fin. (As previously

noted, those portions of the squared-off tube that do not interact with the fin have not been included in this study.) Perhaps the most reasonable heat loss to take for this purpose is that portion of the base-surface emission that streams directly out to space. For example, if the base surface emission for the open-sandwich configuration (fig. 1(b)) is $2\left(\sigma T_b^4 h\right)$, then the portion Q_b^* that would go directly to space is

$$Q_b^* = 2\left(\sigma T_b^4 h\right) F_{1-s} \tag{36}$$

where F_{1-s} is the angle factor from one of the base surfaces (say, base surface 1) to space.

In the closed-sandwich configuration (fig. 1(a)) those parts of the base surface that interact with the fins are internal to the system. So, for this case, F_{1-s} would be identically zero. Thus, the superposition discussed previously cannot be applied to the closed-sandwich configuration.

For the open-sandwich configuration, the base surface contribution Q_b^* to the superposition is given by equation (36). In dimensionless form, this becomes

$$Q_b^*/4L\sigma T_b^4 = \left(\frac{h}{2L}\right) F_{1-s} \tag{36a}$$

By angle factor algebra, F_{1-s} is related to the F_{1-2}, as given by equation (27), as follows:

$$F_{1-s} = \frac{1}{2}\left(1 - F_{1-2}\right) \tag{37}$$

Equation (36a) is to be added to the results for the single, noninteracting fin that are represented by the $L/h = \infty$ curve of figure 6. The actual superposition has been carried out in figure 12(a), where results are shown only for selected values of L/h to preserve clarity. The solid curves are the results that previously appeared in figure 6, while the dashed curves are those obtained by the superposition. The figure indicates that the heat-loss results predicted by the superposition method are, on the one hand, low at large values of N_c and are, on the other hand, high at small values of N_c. Indeed, for $N_c = 0$, the superposition method would predict an ordinate value that would exceed unity by an amount equal to the right side of equation (36a). Further, there is no reason to believe that, for L/h values exceeding 5, the results from the superposition method may not fall high even for large N_c. From an overall appraisal of figure 12(a), it may be

concluded that the superposition method applied here is not satisfactory for practical calculation purposes, at least for the open-sandwich configuration.

The same type of superposition has been attempted for the central-fin configuration. The base surface contribution is given by equations (36a) and (37) as before, but now the appropriate expression for F_{1-2} is equation (35b). A comparison of the heat-transfer predictions from the superposition method with those of the numerical solutions is shown in figure 12(b). The general characteristics of the comparison are very similar to those of figure 12(a), except that now the dashed curve lies above the solid curve for $L/h = 5$. The general conclusions relating to the practical utility of the superposition method remain as previously stated.

CONCLUDING REMARKS

The foregoing analysis has provided results for radiator finned-tube configurations in which the tubes have been idealized as having squared-off exterior surfaces. It would be expected, however, that the squaring off will not have a decisive effect on the heat-transfer results in the L/h range of practical interest (i.e., larger L/h).

An important contribution of this study relates to the conclusions that follow from comparisons among the results. Such comparisons on the basis of equal fin weight show that, for aspect ratios and N_c values of practical interest, the heat-transfer performance does not differ appreciably among the various configurations that have been studied. In the practical range of L/h, it is not expected that the essence of this conclusion will be altered when round tubes (rather than squared-off tubes) and highly emissive nonblack surfaces are used. Under the condition of equal tube weight, it follows that optimizations worked out for one of the configurations should apply to the others.

On the basis of the aforementioned comparison, if tube-portion weights are comparable, it would appear that other factors that are not related to heat transfer may ultimately fix the choice of the fin and tube configuration. Another utility of the present report relates to the presentation of a correct method of approach, both for black and for nonblack surfaces.

Heat Transfer Laboratory
Department of Mechanical Engineering
University of Minnesota
Minneapolis, Minn.
July 10, 1962

APPENDIX - ANALYSIS FOR NONBLACK SURFACES

Consideration will be given here to the derivation of equations governing energy transport in the closed-sandwich configuration. The corresponding equations for the other configurations can be derived from those of the closed sandwich in a manner identical to that employed in the body of the report. Therefore, the other configurations will not be treated here.

The radiant energy leaving a nonblack surface consists not only of emission, but also includes the reflected portion of the incident radiation. For diffuse reflection and emission at a surface, the reflected and emitted energies have the same directional distributions, and no distinction need be made between them. It is therefore convenient to define a new energy quantity, the radiosity B, as the sum of the emitted and reflected energies per unit time and area:

$$B = \epsilon\sigma T^4 + \rho H \tag{A1}$$

where H is the incident energy per unit time and area. For a gray surface, the reflectivity ρ is equal to $(1 - \epsilon)$, and additionally $\alpha = \epsilon$.

By utilizing the radiosity, the analysis previously given for the black-surfaced, closed-sandwich configuration can be readily generalized. It will be assumed here for simplicity that all surfaces are gray and have the same emissivity, but the latter restriction can be lifted without difficulty. The energy balance (eq. (2)) on an elementary volume of fin as shown in figure 2 continues to apply, as does the net conduction given by equation (3). The net radiation is equal to the difference between the energy emitted and energy absorbed. The emitted energy is $\left[\epsilon\sigma T^4(x)\right] 2\, dA_x$, while the absorbed radiation is $\alpha H(x) dA_x$. With this, the expression for the net radiation is

$$\left(dQ_{net}\right)_{rad} = \epsilon\left[2\sigma T^4(x) - H(x)\right] dA_x \tag{A2}$$

The incident energy $H(x)$ comes from two distinct zones as before: (1) from the opposite fin and (2) from the base surfaces. The first of these contributions has essentially the same mathematical representation as before, except that the emissive power $\sigma T^4(y)$ is replaced by the radiosity $B(y)$. Thus, the generalization of equation (5) applicable to nonblack surfaces is

$$dA_x \int_{y=0}^{2L} B(y) dF_{dA_x - dA_y} \tag{A3}$$

The contribution of the base surfaces to $H(x)$ must be considered in somewhat greater detail. Whereas an isothermal black surface has uniform emissive power, it is not necessarily true that an isothermal nonblack surface has uniform radiosity. In general, the radiosity on such a surface will not be uniform. Thus, for the case of nonblack surfaces, it is necessary to find the contribution to $H(x)$ from each element of base surface and then integrate to find the total contribution. This is identical to the procedure employed in deriving expression (5). Proceeding along the same lines, but replacing emissive powers by radiosities, the contribution of the base surfaces to $H(x)$ is found to be

$$dA_x \left[\int_{z_1=0}^{h} B(z_1) dF_{dA_x - dA_1} + \int_{z_2=0}^{h} B(z_2) dF_{dA_x - dA_2} \right] \tag{A4}$$

The radiosities $B(z_1)$ and $B(z_2)$ are equal when $z_1 = z_2$ because of symmetry.

The incident energy $H(x)$ is the sum of expressions (A3) and (A4). These may be employed to evaluate equation (A2) for the net radiation at dA_x. With this and with the net conduction from equation (3), the heat balance (eq. (2)) becomes

$$\frac{kt}{\epsilon} \frac{d^2T}{dx^2} = 2\sigma T^4 - \int_{y=0}^{2L} B(y) dF_{dA_x - dA_y}$$

$$- \left[\int_{z_1=0}^{h} B(z_1) dF_{dA_x - dA_1} + \int_{z_2=0}^{h} B(z_2) dF_{dA_x - dA_2} \right] \tag{A5}$$

It is convenient to introduce dimensionless variables X, Y, and θ as defined by equation (9), and in addition

$$\beta = B/\sigma T_b^4 \qquad Z_1 = z_1/h \qquad Z_2 = z_2/h \tag{A6}$$

Also, because of symmetry $B(y) = B(2L - y)$, $B(z_1) = B(z_2)$, $B(z_1) = B(h - z_1)$. Incorporating all this into equation (A5), there is obtained

$$\frac{1}{\epsilon(N_c)_L}\frac{d^2\theta}{dX^2} = 2\theta^4 - \left\{ \frac{\left(\frac{h}{L}\right)^2}{2}\int_0^1 \beta(Y)dY \left[\frac{1}{\left[(Y - X)^2 + \left(\frac{h}{L}\right)^2\right]^{3/2}} \right.\right.$$

$$\left. + \frac{1}{\left[(2 - Y - X)^2 + \left(\frac{h}{L}\right)^2\right]^{3/2}} \right] + \frac{\left(\frac{h}{L}\right)^2}{2}\int_0^{1/2} \beta(Z_1)dZ_1 \left[\frac{XZ_1}{\left[X^2 + Z_1^2\left(\frac{h}{L}\right)^2\right]^{3/2}} \right.$$

$$+ \frac{X(1 - Z_1)}{\left[X^2 + \left(\frac{h}{L}\right)^2(1 - Z_1)^2\right]^{3/2}} + \frac{(2 - X)Z_1}{\left[(2 - X)^2 + \left(\frac{h}{L}\right)^2 Z_1^2\right]^{3/2}}$$

$$\left.\left. + \frac{(2 - X)(1 - Z_1)}{\left[(2 - X)^2 + \left(\frac{h}{L}\right)^2(1 - Z_1)^2\right]^{3/2}} \right] \right\} \qquad \text{(A7)}$$

in which the angle factors between dA_x and dA_1 and between dA_x and dA_2 have been evaluated by application of equation (12) with dy replaced by dz. The boundary conditions on θ remain as stated in equation (11).

Inspection of equation (A7) reveals that there are three unknown functions: the temperature distribution $\theta(X)$ and the radiosity distributions $\beta(Y)$ and $\beta(Z)$. Two additional relations between the unknowns are therefore required. These relations may be derived by making use of the radiosity equation (A1). First, applying this to the location

x and noting that the incident flux $H(x)/\sigma T_b^4$ is given by the quantity within the braces on the right side of equation (A7), there follows

$$\beta(X) = \epsilon\theta^4 + (1 - \epsilon)\left\{\text{Terms within braces of eq. (A7)}\right\} \qquad \text{(A8)}$$

Because of symmetry, $\beta(X) = \beta(Y)$ when $X = Y$. So, $\beta(X)$ and $\beta(Y)$ are the same functions; only the independent variables have been interchanged. It then follows that equation (A8) is essentially an integral equation for $\beta(X)$. An additional relation between the unknowns is obtained by applying the radiosity equation to a surface element on one of the base surfaces. After evaluating the incident radiation from the fins and the opposite base surface, equation (A1) becomes

$$\beta(Z_1) = \epsilon + \frac{(1 - \epsilon)}{2}\left\{4\left(\frac{L}{h}\right)^2\int_0^{1/2}\beta(Z_2)dZ_2\left[\frac{1}{\left[(Z_2 - Z_1)^2 + 4\left(\frac{L}{h}\right)^2\right]^{3/2}}\right.\right.$$

$$\left. + \frac{1}{\left[(1 - Z_2 - Z_1)^2 + 4\left(\frac{L}{h}\right)^2\right]^{3/2}}\right] + \left(\frac{h}{L}\right)\int_0^1 \beta(X)dX\left[\frac{XZ_1}{\left[X^2 + \left(\frac{h}{L}\right)^2 Z_1^2\right]^{3/2}}\right.$$

$$+ \frac{(2 - X)Z_1}{\left[(2 - X)^2 + \left(\frac{h}{L}\right)^2 Z_1^2\right]^{3/2}} + \frac{X(1 - Z_1)}{\left[X^2 + \left(\frac{h}{L}\right)^2 (1 - Z_1)^2\right]^{3/2}}$$

$$\left.\left. + \frac{(2 - X)(1 - Z_1)}{\left[(2 - X)^2 + \left(\frac{h}{L}\right)^2 (1 - Z_1)^2\right]^{3/2}}\right]\right\} \qquad \text{(A9)}$$

Because of symmetry, $\beta(Z_1) = \beta(Z_2)$ when $Z_1 = Z_2$. So, $\beta(Z_1)$ and $\beta(Z_2)$ are the same functions; only the independent variables have been interchanged. Equation (A9) is therefore an integral equation for finding $\beta(Z_1)$.

The governing equations for the energy transfer in the closed-sandwich configuration with nonblack surfaces are embodied in (A7), (A8), and (A9). Simultaneous solution of this nonlinear, integro-differential system is required to determine the heat-transfer characteristics. By comparing this mathematical system with equation (17), it is clear that the consideration of nonblack surfaces adds a computational complexity to the problem in addition to new unknowns and parameters.

REFERENCES

1. Lieblein, Seymour: Analysis of Temperature Distribution and Radiant Heat Transfer Along a Rectangular Fin. NASA TN D-196, 1959.

2. Bartas, J. G., and Sellers, W. H.: Radiation Fin Effectiveness. Jour. Heat Transfer, ser. C, vol. 82, no. 1, Feb. 1960, pp. 73-75.

3. Callinan, J. P., and Berggren, W. P.: Some Radiator Design Criteria for Space Vehicles. Jour. Heat Transfer, ser. C, vol. 81, no. 3, Aug. 1959, pp. 237-244.

4. Diamond, P. M., and Hopson, G. D.: Heat Rejection in Space. Pt. 5 of Short Course in Space Power Plants, Univ. Calif., July 1961. (See also Rep. AT-4, Convair.)

5. Sparrow, E. M., and Eckert, E. R. G.: Radiant Interaction Between Fin and Base Surfaces. Jour. Heat Transfer, ser. C, vol. 84, no. 1, Feb. 1962, pp. 12-18.

6. Jakob, Max: Heat Transfer. Vol. 2. John Wiley & Sons, Inc., 1957.

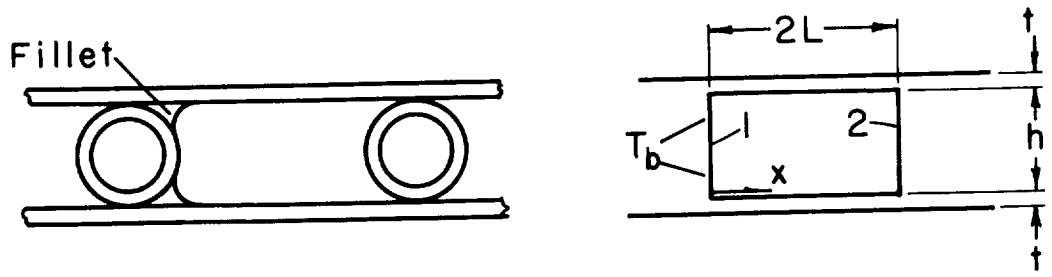

(a) Closed sandwich.

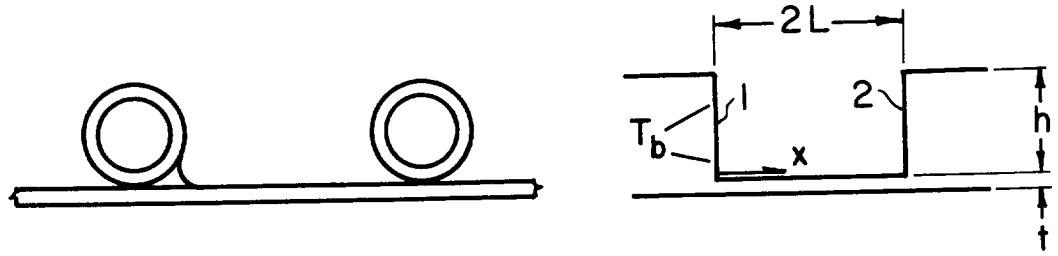

(b) Open sandwich.

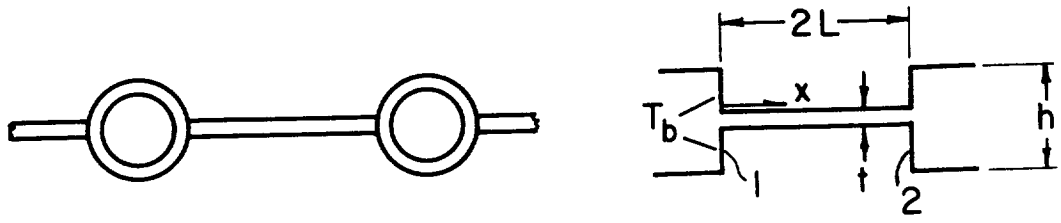

(c) Central fin.

Figure 1. - Radiator finned-tube configurations.

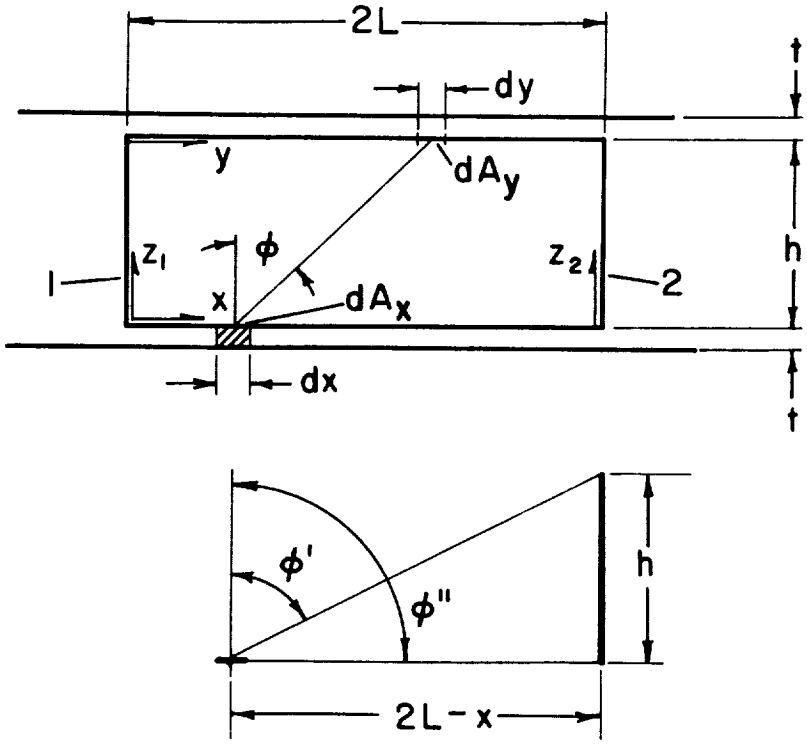

Figure 2. - Diagram for analysis of closed-sandwich configuration.

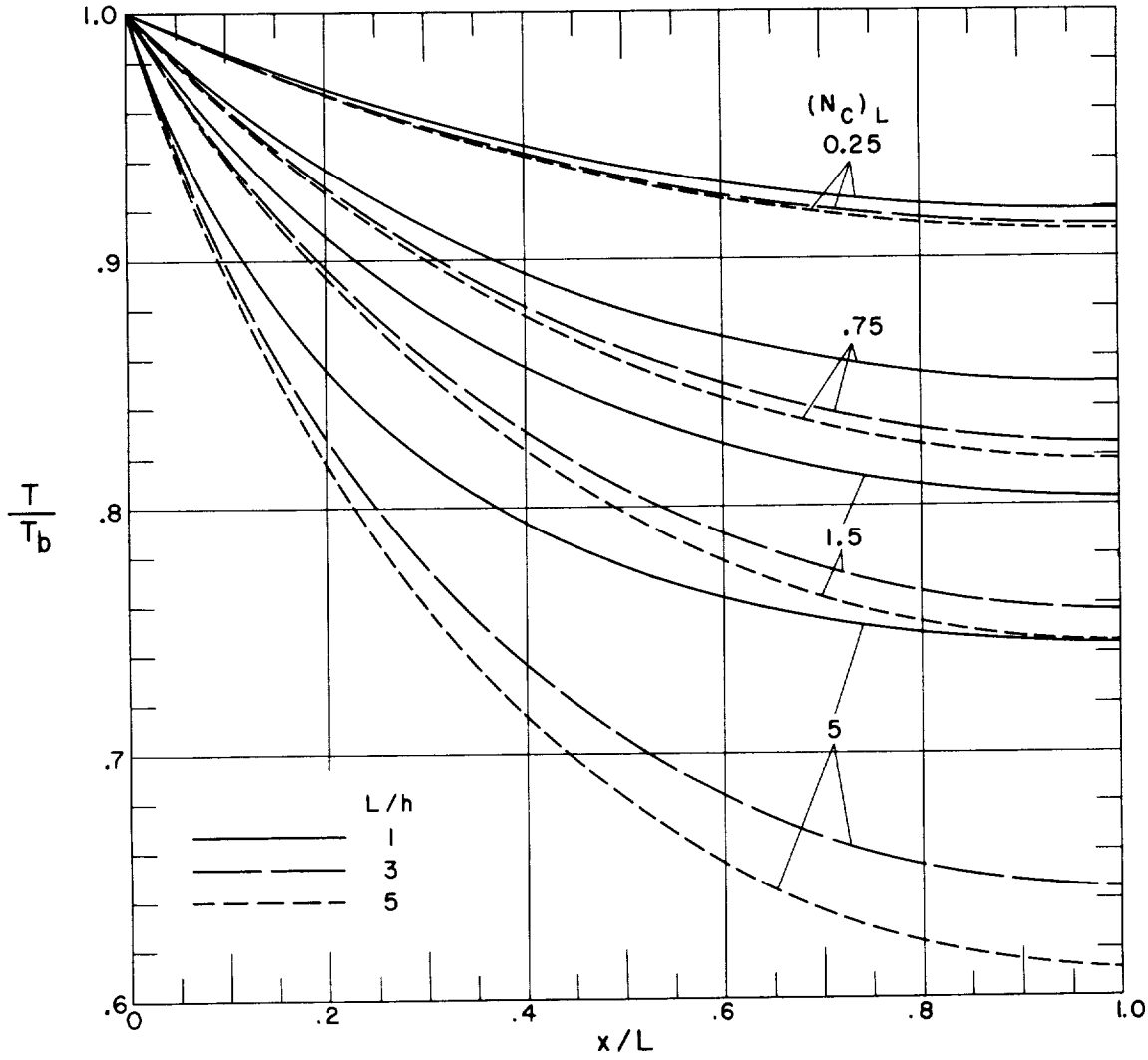

(a) Closed-sandwich configuration.

Figure 3. - Representative fin temperature profiles.

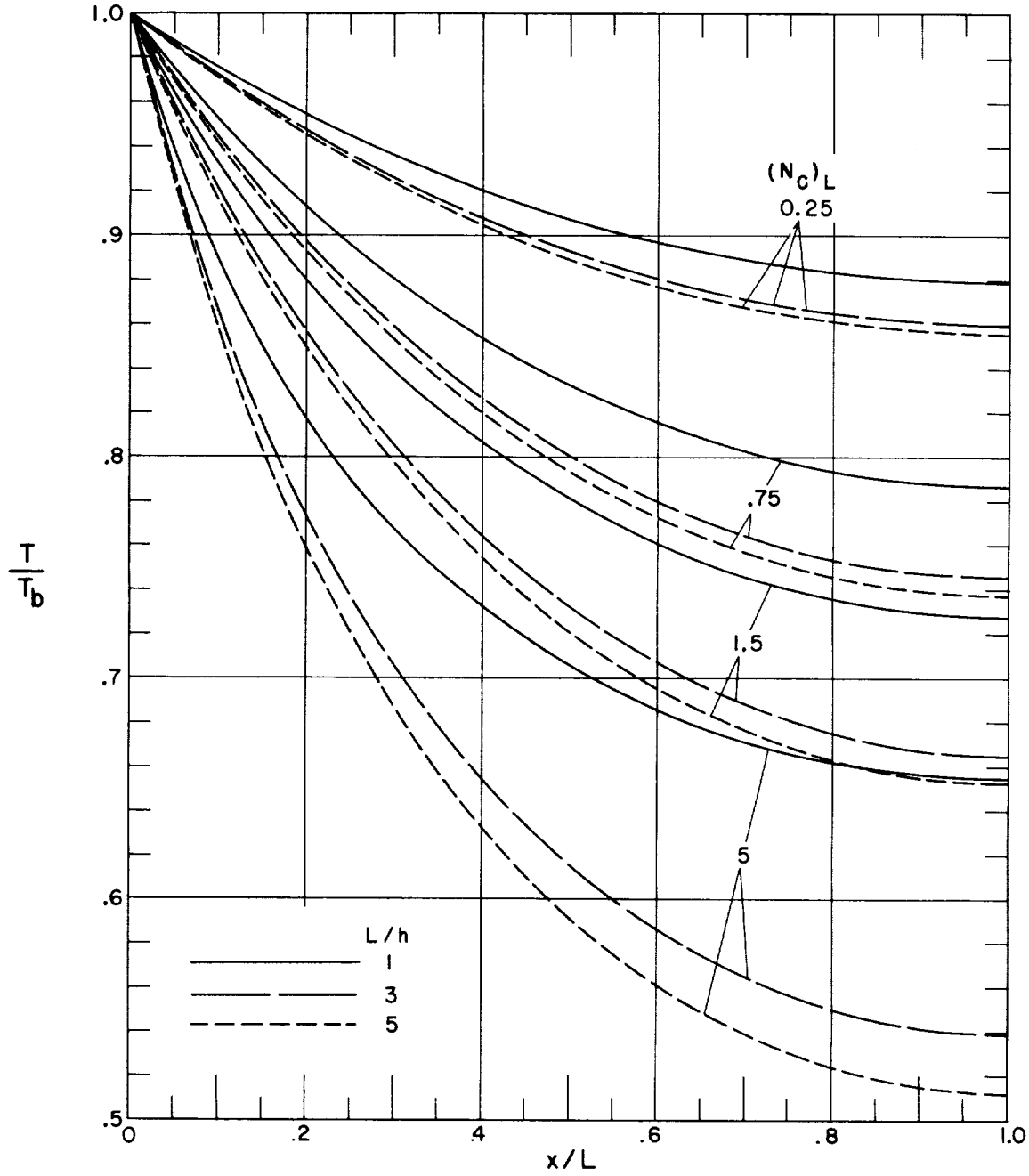

(b) Open-sandwich configuration.

Figure 3. - Continued. Representative fin temperature profiles.

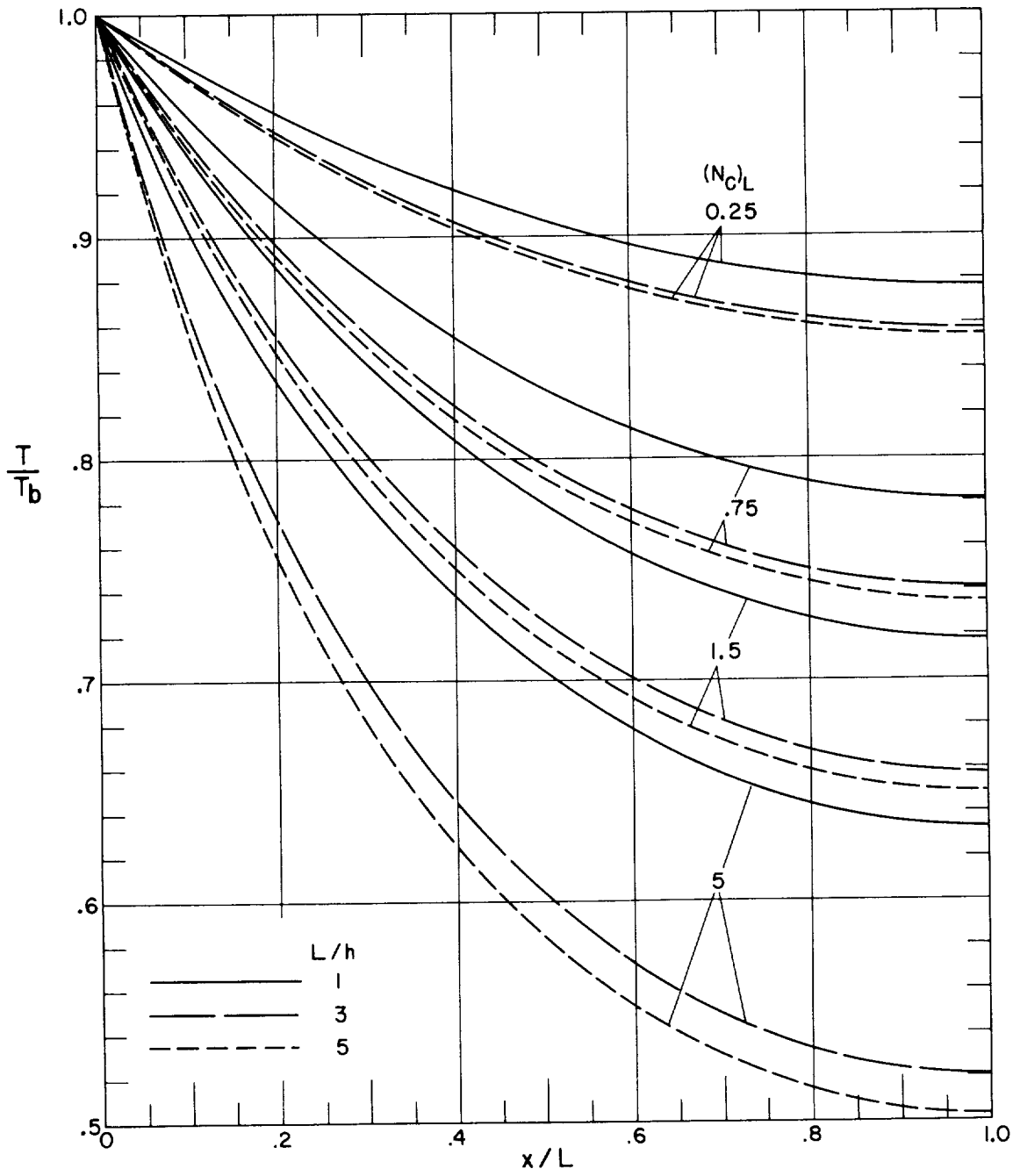

(c) Central-fin configuration.

Figure 3. - Concluded. Representative fin temperature profiles.

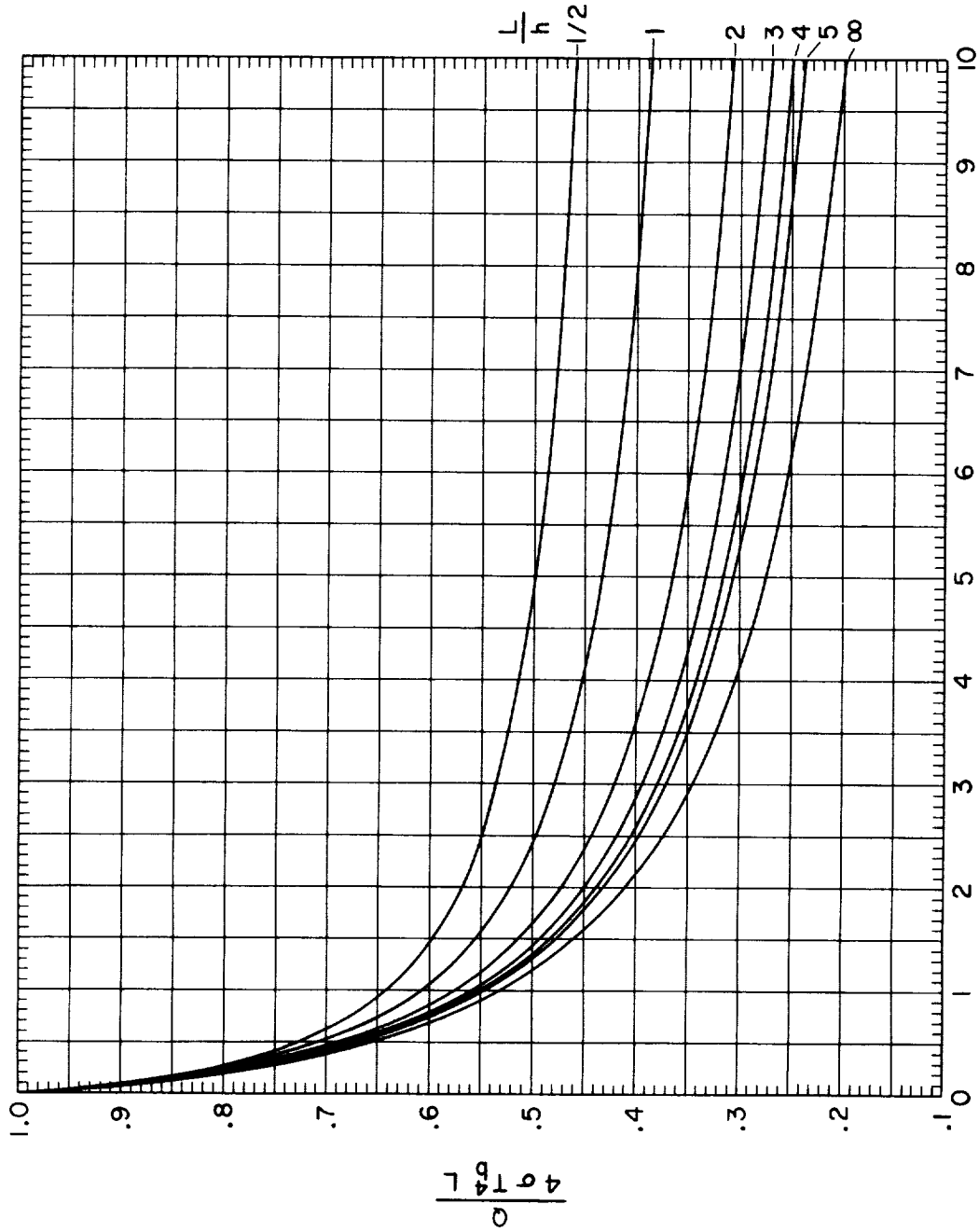

Figure 4. - Heat-loss results for closed-sandwich configuration.

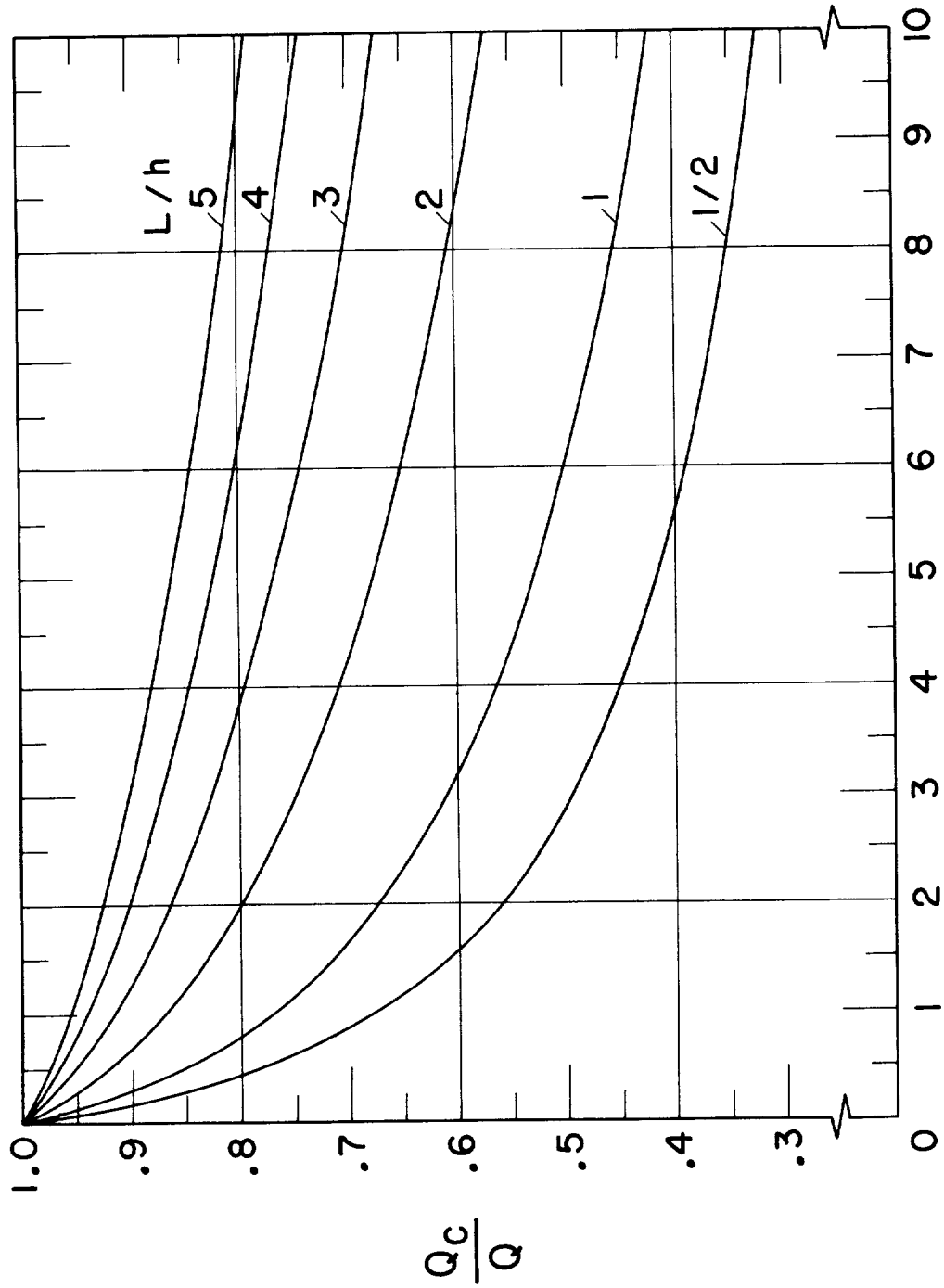

Figure 5. - Heat loss due to conduction in fin relative to total heat loss. Closed-sandwich configuration.

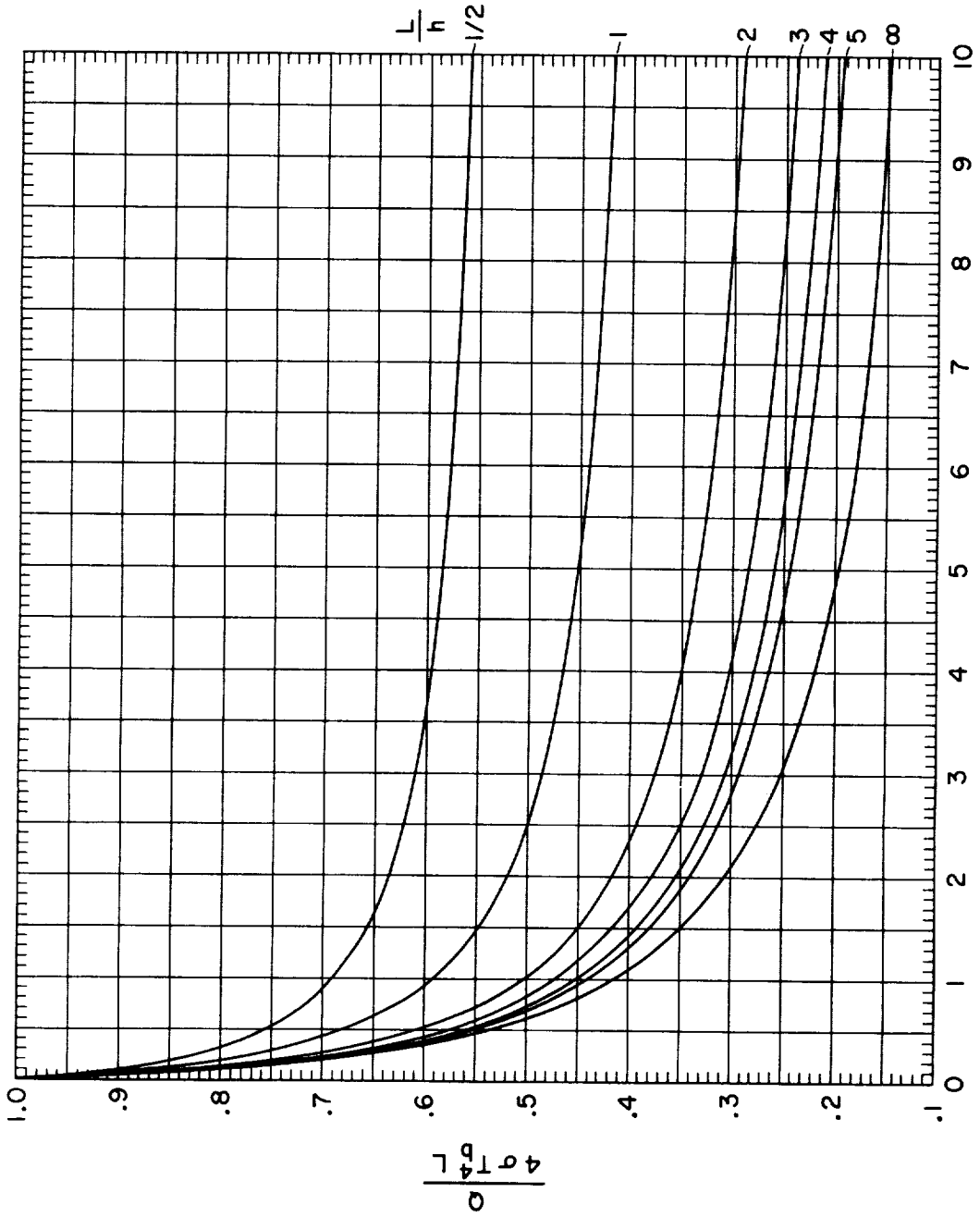

Figure 6. - Heat-loss results for open-sandwich configuration.

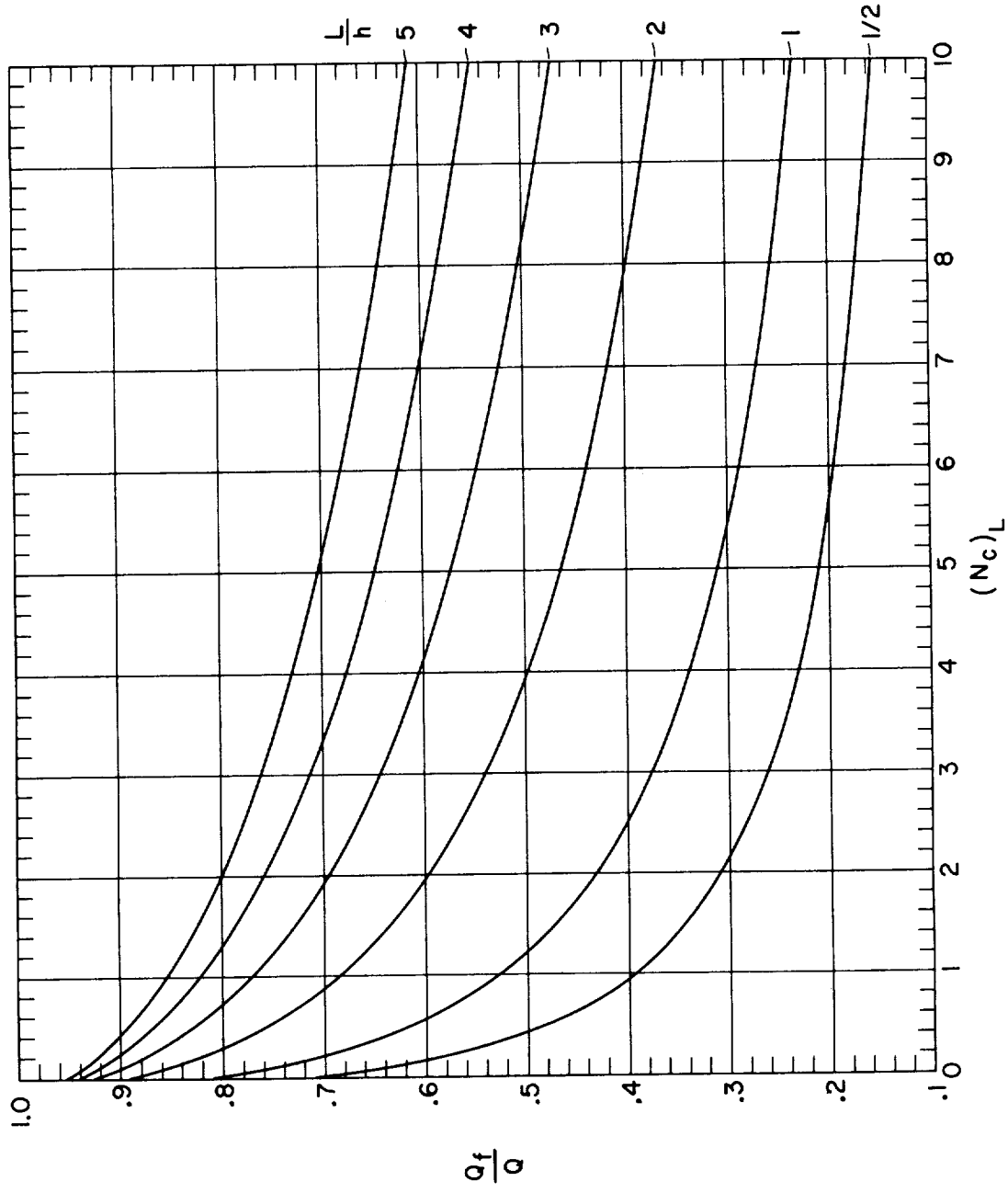

Figure 7. - Fin heat loss relative to total heat loss. Open-sandwich configuration.

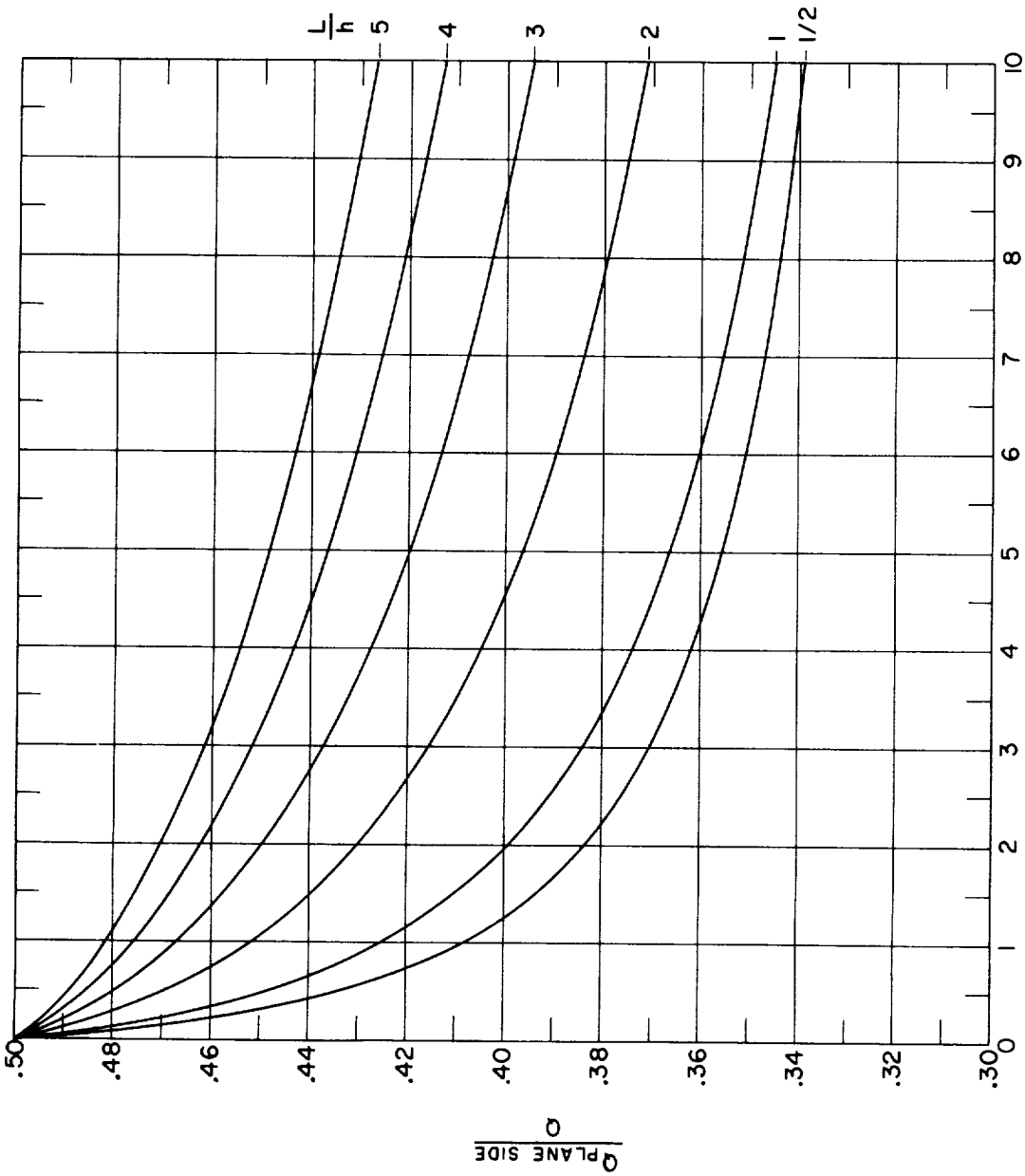

Figure 8. - Heat loss from plane side relative to total heat loss. Open-sandwich configuration.

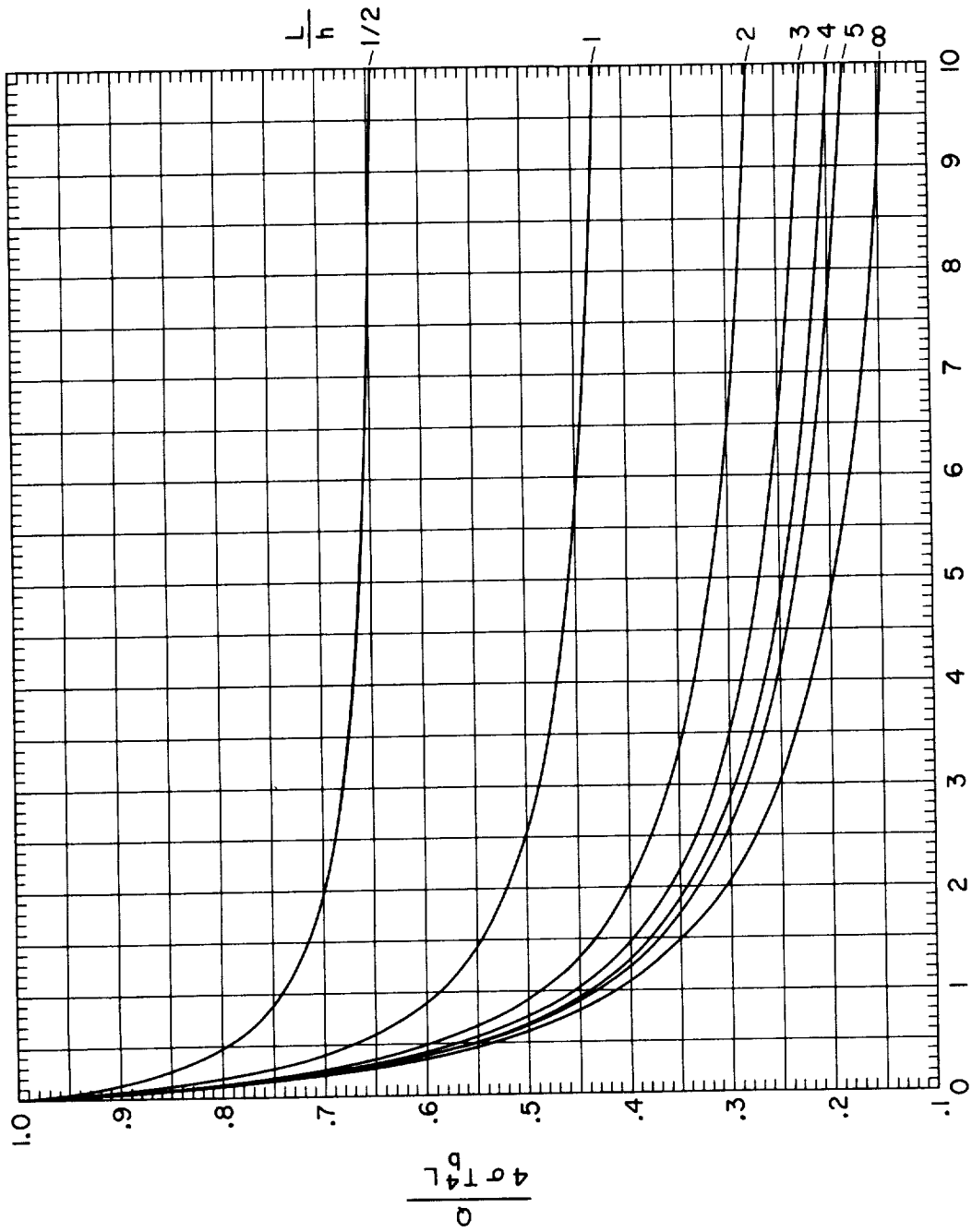

Figure 9. - Heat-loss results for central-fin configuration.

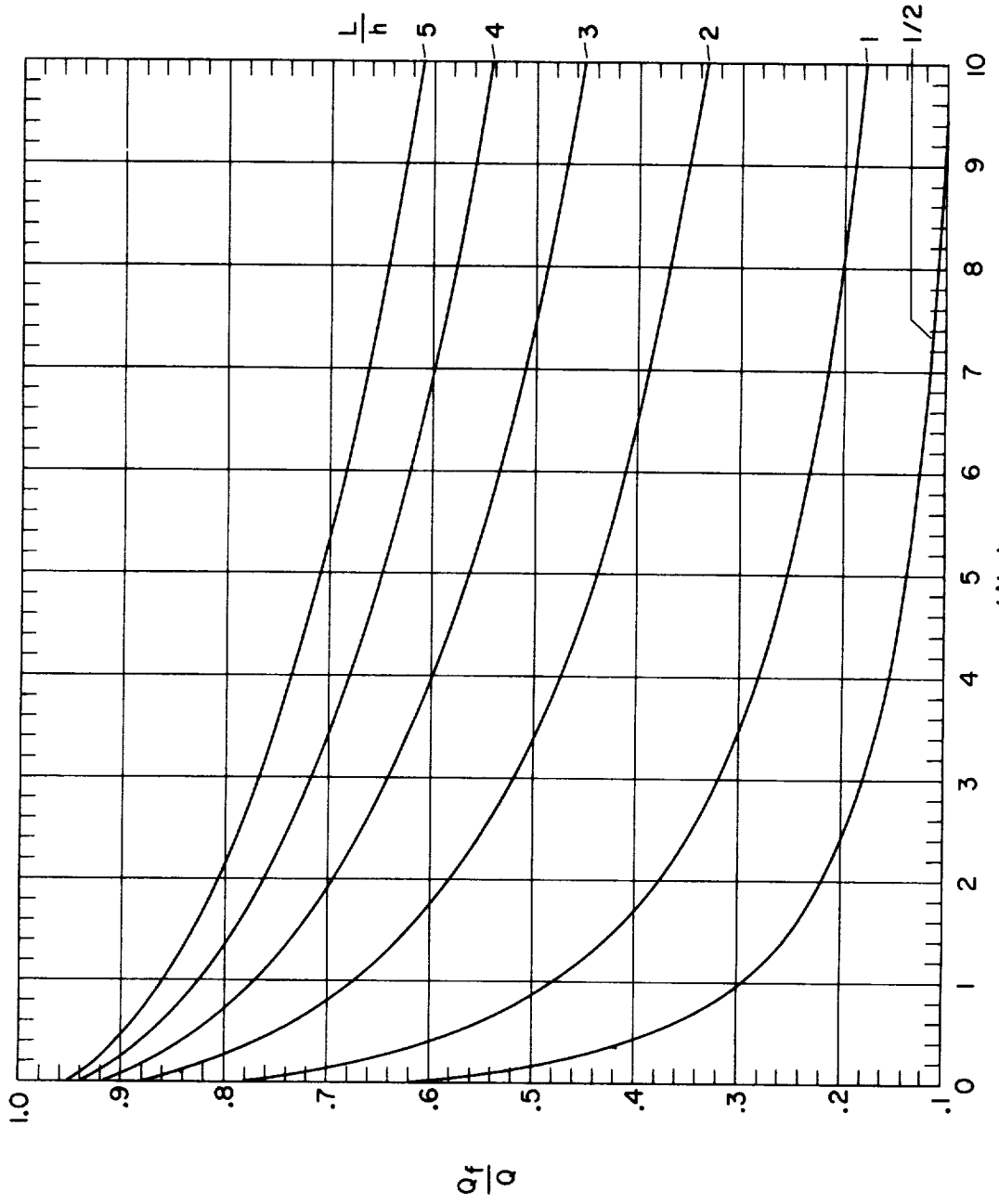

Figure 10. - Fin heat loss relative to total heat loss. Central-fin configuration.

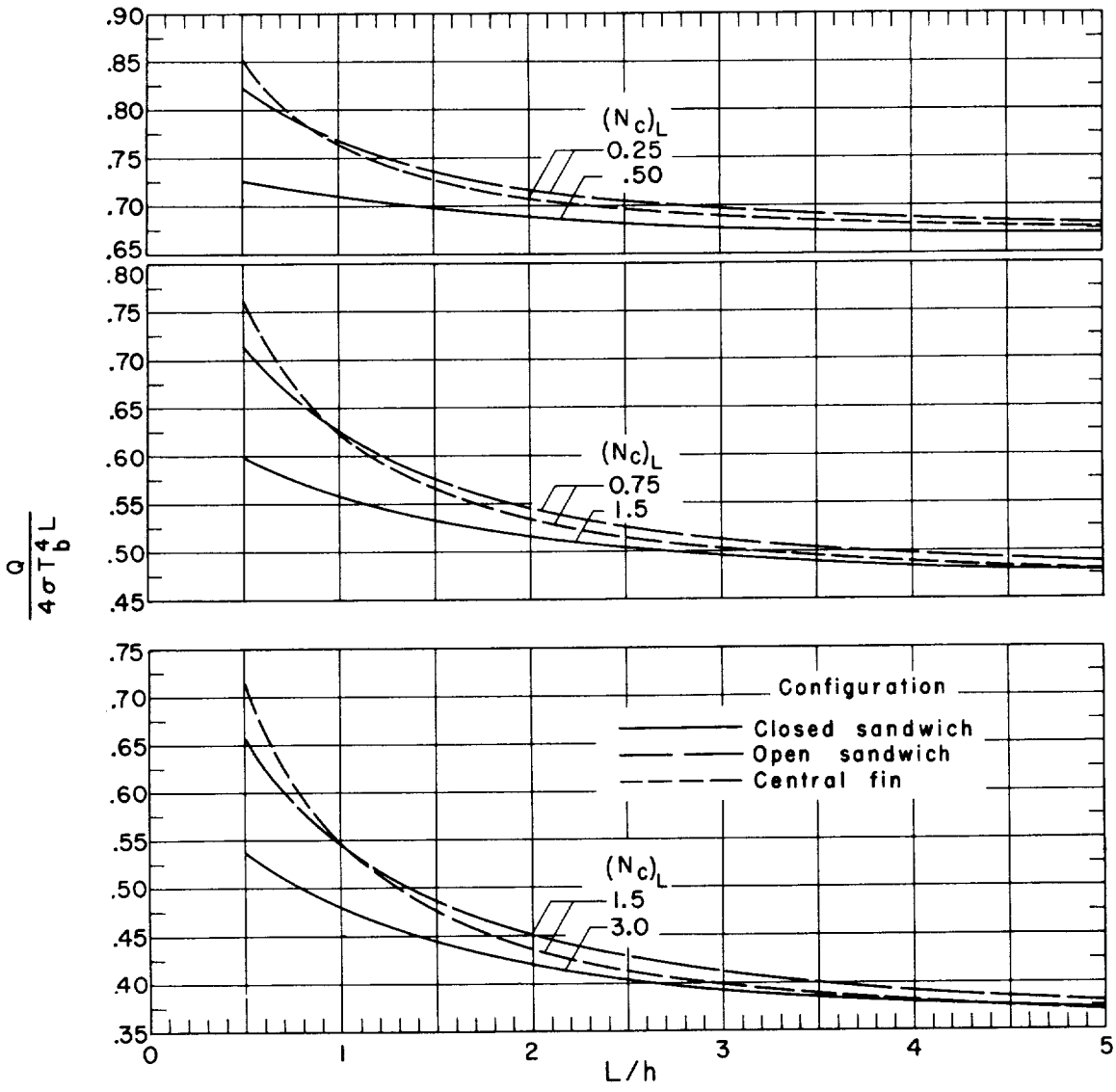

(a) Range of small $(N_c)_L$.

Figure 11. - Heat-loss comparison on the basis of equal fin weight.

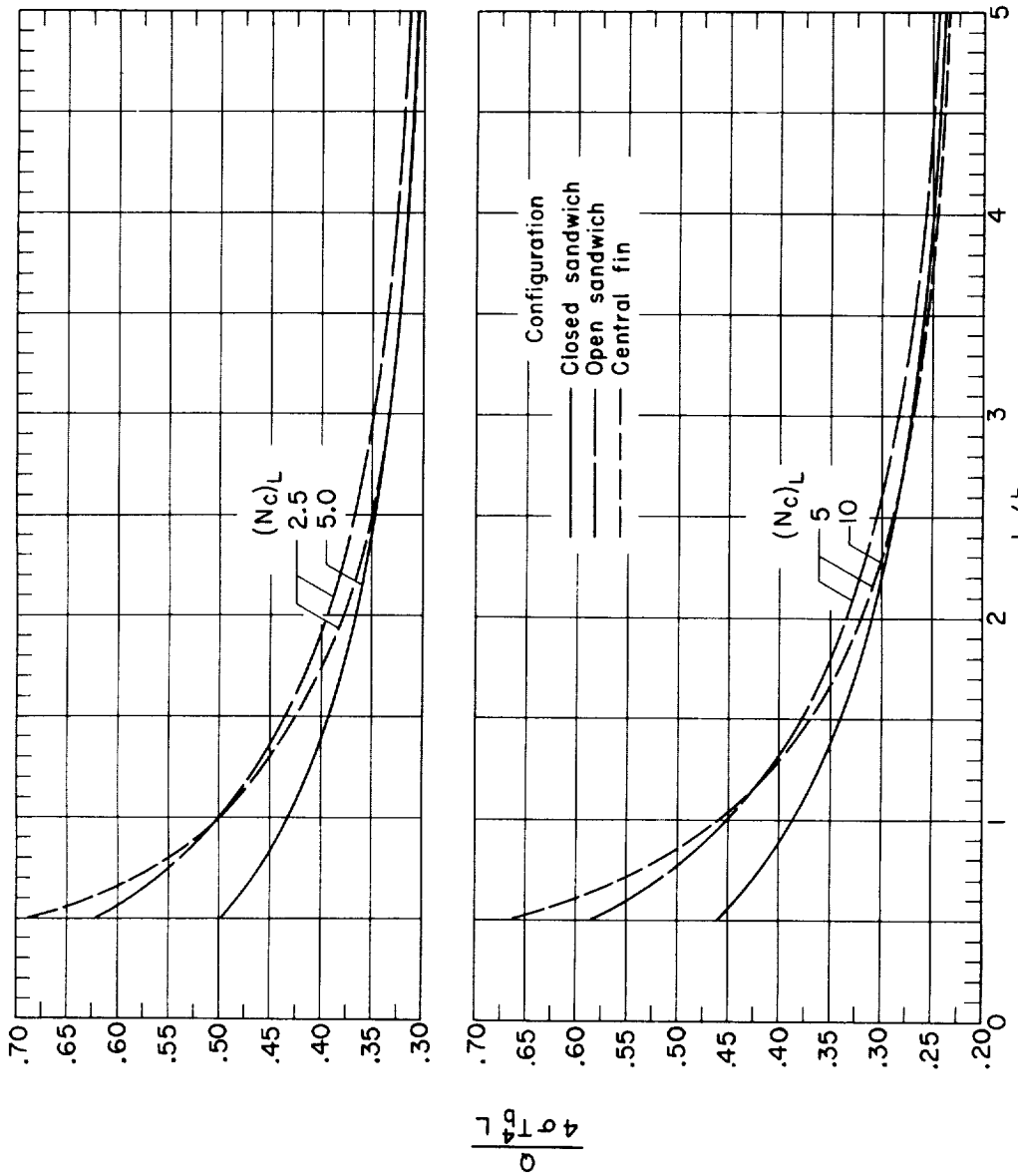

(b) Range of large $(N_c)_L$.

Figure 11. - Concluded. Heat-loss comparison on the basis of equal fin weight.

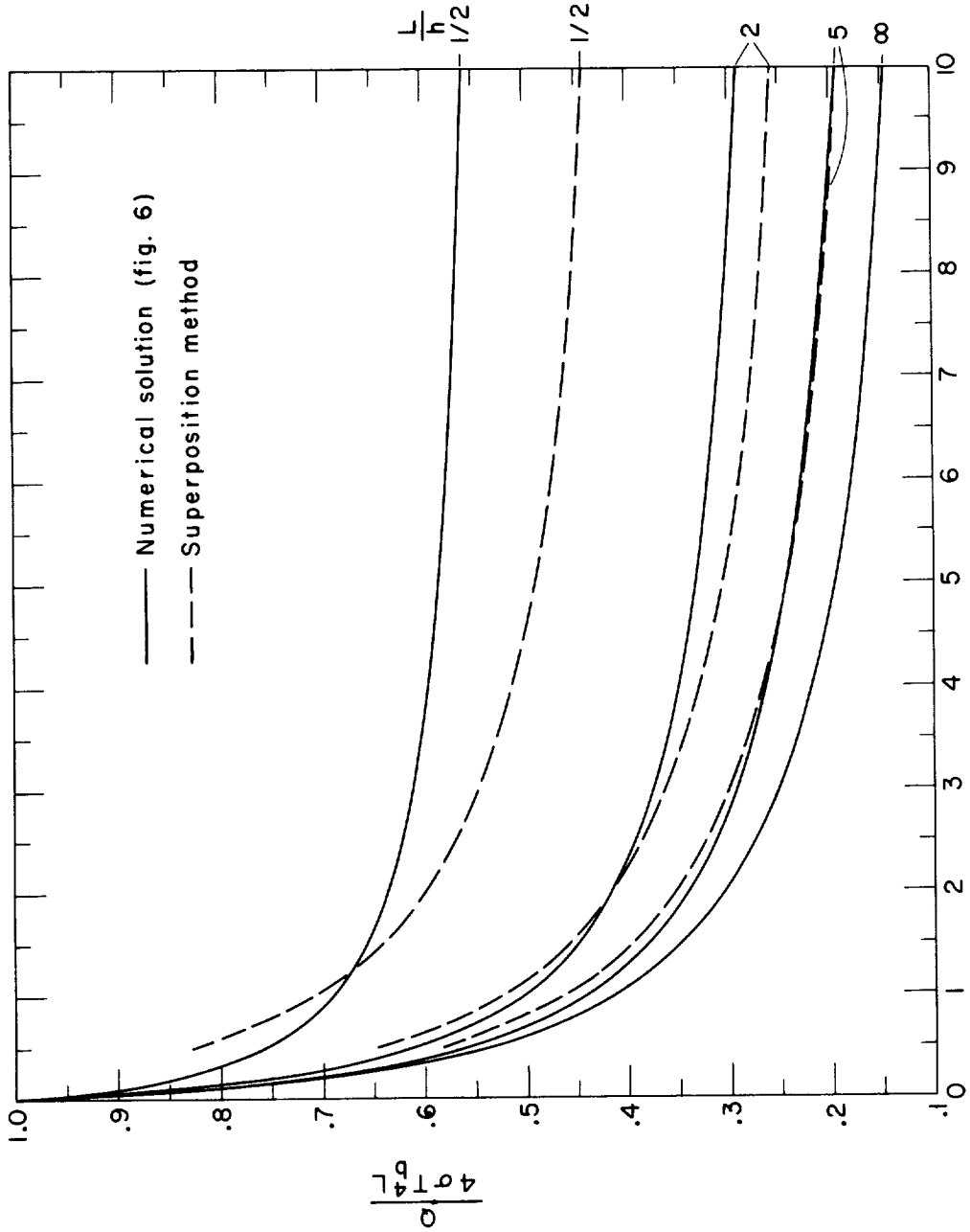

(a) Open-sandwich configuration.

Figure 12. - Comparison of results from superposition method and from numerical solutions.

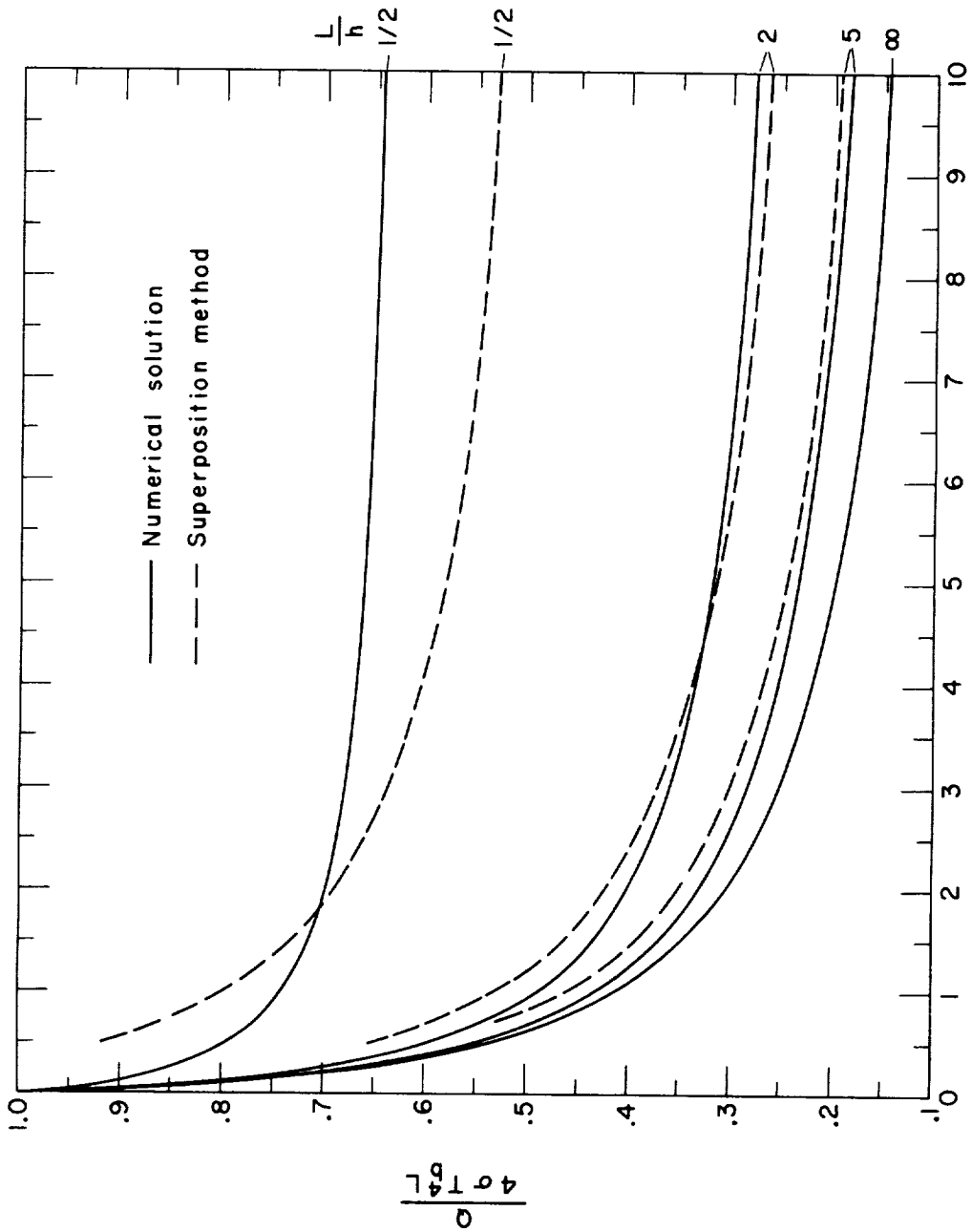

(b) Central-fin configuration.

Figure 12. - Concluded. Comparison of results from superposition method and from numerical solutions.